Contrib Mineral Petrol (2011) 162:479–500
DOI 10.1007/s00410-011-0607-6

ORIGINAL PAPER

U-Pb thermochronology: creating a temporal record of lithosphere thermal evolution

Terrence Blackburn · Samuel A. Bowring · Blair Schoene · Kevin Mahan · Francis Dudas

Received: 26 June 2010 / Accepted: 3 January 2011 / Published online: 26 January 2011

Abstract A new approach to U-Pb accessory mineral thermochronology allows high-resolution time-temperature histories to be extracted from lower crustal xenoliths. The combination of the U-Pb system's dual decay scheme with the effects of temperature dependent Pb-diffusion can yield a time sensitive record of Pb production/diffusion within accessory phases. The difference in half-life for parent isotopes ^{238}U and ^{235}U results in the time-variable production of Pb isotopes ^{206}Pb and ^{207}Pb, while Pb diffusion can result in large variations in the time-scales at which Pb retention occurs between grains of different sizes. The combined effects of variable production rates between the two systems and diffusion result in data topologies on a concordia diagram that permit distinction between slow cooling and reheating t-T paths. In slowly cooled systems, the difference in time for Pb retention for grains of variable size yields a measure of partial retention zone (PRZ) residence time, and provides a robust measure of cooling rate through the PRZ. In Montana, three lower crustal xenoliths, each from a different depth, yield U-Pb rutile data that record a prolonged (>1 Ga) and slow cooling history towards a steady state geothermal gradient following the amalgamation of the terrain onto North America. The shallowest samples record the initial recovery of a conductive geothermal gradient and cool through the mineral PRZ at rates of <0.25°C/Ma over ~500 Ma. Deeper xenoliths record cooling at younger times over similar time scales and rates. This multi-depth thermal history provides a long-term record of lithosphere cooling and stabilization.

Keywords U-Pb · Thermochronology · Lithosphere · Thermal evolution · Lower crust · Xenoliths · Rutile

Communicated by T. L. Grove.

Electronic supplementary material The online version of this article (doi:10.1007/s00410-011-0607-6) contains supplementary material, which is available to authorized users.

T. Blackburn (✉) · S. A. Bowring · F. Dudas
Massachusetts Institute of Technology, EAPS, 77 Massachusetts Ave MIT Bldg 54-1117, Cambridge, MA 02139, USA
e-mail: Terrence@mit.edu

B. Schoene
Department of Geosciences, Princeton University, 219 Guyot Hall, Princeton, NJ 08544, USA

K. Mahan
Department of Geological Sciences, University of Colorado-Boulder, 2200 Colorado Ave., Campus Box 399, Boulder, CO 80309, USA

Introduction

Over the past 20 years thermochronologic techniques including U-Pb, Rb-Sr, K-Ar, ^{40}Ar/^{39}Ar, fission track and (U-Th)/He systems have allowed earth scientists to accurately describe the time-temperature evolution of rock samples. The diffusive loss of daughter isotopes in these systems can be quantified by volume-diffusion theory and exploited as a reliable method to yield temperature sensitive dates. Low-temperature (<400–60°C) thermochronometric systems, such as ^{40}Ar/^{39}Ar and (U-Th)/He have typically been applied to structural, tectonic and geomorphologic studies of the upper crust with the goal of constraining near-surface thermal histories. Reconstructing a samples thermal history can be used to quantify heat transfer mechanisms operating within the lithosphere, providing a time-dependent measure for this process.

In contrast to noble gas thermochronology, U-Pb accessory phase thermochronometry (minerals: apatite, titanite and rutile) allows estimates of cooling rates of rocks as they pass through moderate to high temperatures (400–800°C) corresponding to thermal histories for rocks between 20 and 50 km depth. Most attempts to employ U-Pb thermochronometers have produced dates consistent with exhumation of post-peak metamorphic lower crustal terranes (Baldwin et al. 2004; Flowers et al. 2006). Schmitz et al. (2003), however, applied U-Pb accessory phase thermochronology to explore the thermal relaxation of ancient cratonic lithosphere by dating rutile, titanite and apatite from exhumed lower crustal xenoliths. Lower crustal xenoliths may preserve ancient cooling histories, from the high temperatures during and following igneous crystallization and/or metamorphism (700–1,000°C), to the low temperatures predicted for a steady state geotherm in the lower crust (ca 450–550°C). This history is initially recorded by high temperature geochronometers such as zircon or monazite, while cooling is recorded by moderate temperature thermochronometers apatite, rutile and titanite. Archean cratons are characterized by thick (>200 km) lithospheric mantle of depleted peridotite that effectively insulate the crust from thermal and tectonic perturbations (e.g. Jordan 1988). Though the antiquity of the crust and keels is well established, the time-scales of cooling and stabilization of these cratons is poorly understood. U-Pb thermochronology of lower crustal xenoliths can be used to constrain the long-term thermal relaxation of these tectonic terranes, and potentially decipher the magnitude of heat transfer mechanisms operating over the history of a craton.

An additional contrast between U-Pb and noble gas thermochronology is the U-Pb system's dual decay scheme, where two parent isotopes, ^{238}U and ^{235}U, decay to daughter isotopes ^{206}Pb and ^{207}Pb respectively. The difference in decay rates between parent isotopes imposes a time-variant parent and daughter isotopic composition for any point in Earth's history. Volume diffusion behavior, in particular for slowly cooled systems, induces age gradients within single grains and among grains of varying size as a result of partial retention of radiogenic daughter and diffusion's length-scale dependency. This results in the retention of Pb between grains of different sizes over different time-scales, with each grain acquiring a unique parent-daughter ratio and daughter isotopic composition. The dual decay scheme can be exploited as two separate thermochronologic systems that when combined, can yield data that is unique to a particular cooling path. This is a distinct advantage over single isotope systems that are often plagued by non-unique data sets in particular the ambiguity of potentially identical internal diffusion profiles and grain size-age relationships that can be produced by slow-cooling and reheating time-temperature (t-T) paths.

The purpose of this paper to is to: (1) outline new numerical and laboratory procedures for U-Pb thermochronology, (2) demonstrate how the U-Pb system's dual decay scheme can yield time sensitive information on Pb diffusion allowing for the determination of unique cooling paths, (3) show how duration in the Pb PRZ affects the topology of U-Pb data plotted on a concordia diagram, which in turn can provide a robust estimate of cooling rate and (4) demonstrate that an approach involving multiple xenolith samples from different depths can further be used to decipher thermal histories for the deep lithosphere.

U-Pb thermochronology

A major goal of radioisotopic thermochronology is to determine an accurate time-temperature history for a sample as it passes through the closure interval of different mineral-isotopic chronometers. Temperature sensitive U-Pb dates are the result of thermally activated volume diffusion of radiogenic Pb that is produced by the decay of U. In order to assign meaningful temperatures to U-Pb dates, we need a quantitative assessment of Pb diffusion behavior within the accessory minerals of interest (rutile, apatite, titanite). This behavior can be approximated by the 1-D diffusion-production equation:

$$\frac{\partial C}{\partial t} = D(T)\frac{\partial^2 C}{\partial r^2} + P \quad (1)$$

where the change in concentration of an element (C) (in this case Pb) with time (t) is equal to the second order spatial derivative of the element concentration multiplied by a Diffusion constant (D), which is itself a function of temperature (T). A production term (P) accounts for the in-situ decay of radiogenically produced daughter. A successful solution to this equation will provide us with a book-keeping method for radiogenically produced ^{206}Pb and ^{207}Pb as it varies within a grain from diffusion (D) and decay of uranium (P) as a function of time.

The variability of both daughter production and daughter retention with temperature and time presents a significant complication in understanding the meaning of measured dates of whole mineral grains. The open versus closed system behavior of elements in solids is dependent upon whether diffusion or production controls the budget of Pb within an accessory phase. Open system behavior occurs at higher temperatures when diffusion is fast enough to induce the loss of radiogenic daughter as quickly as it is produced by decay. Closed system behavior occurs at low temperatures when diffusive loss of Pb is so slow that all radiogenically produced Pb is effectively retained. The region of time-temperature space between open and closed system behavior is defined as the Partial Retention Zone (PRZ), a

region where both production and diffusion are operating at or a near a balance resulting in the partial retention of radiogenic daughter. Any measured U-Pb date, is a result of the daughter isotope gained since the time of system closure plus the daughter acquired in the PRZ. The partial retention of radiogenic daughter is controlled by three different variables, all simultaneously and independently operating to create a unique partial retention zone for a particular thermal history. These variables are: (1) temperature dependent diffusion of radiogenic daughter, (2) production of radiogenic daughter and (3) diffusion's length dependency. This first variable, the diffusion of radiogenic daughter, is controlled by the sample's time-temperature path and results in a unique PRZ for a specific t-T path. For example, fast cooling rates condense the values of diffusivity that may yield partial retention behavior and limit the effects of PRZ residence. Slow cooling, in contrast, results in prolonged time periods with an effective diffusivity that induces partial loss of daughter, yielding a PRZ that is unique to a cooling path. The second key variable, daughter production, will vary both in time as the activity of the parent isotope changes and between different radiometric system. For example, the difference in daughter production rates from the decay of ^{238}U and ^{235}U results in a unique PRZ for the ^{235}U-^{207}Pb and ^{238}U-^{206}Pb systems. Lastly, the length scale dependency of diffusion requires that radiogenic daughter that is produced within the cores of grains has a physically longer distance to travel than the daughter product produced at the edges. The difference in time-scales between Pb-retention in the core and rim of a grain leads to an apparent difference in the time of grain core vs. rim closure while simultaneously providing a temporal record of PRZ residence. For grains of variable size, this length scale-dependency will result in each individual grain size partially retaining Pb over different time periods which in turn results in each grain having its own unique PRZ. The ultimate goal of assigning a meaningful temperature to any measured thermochronometric date requires an understanding for how all of these variables contribute to affect the duration of PRZ residence. The most commonly used method for estimating PRZ residence and assigning a temperature to a measured thermochronologic date is the Dodson method (Dodson 1973).

The Dodson method has been successfully applied to upper-crustal thermochronologic studies, but some of the models inherent assumptions are likely violated in the lower crust. These assumptions include: (1) a monotonic cooling path and (2) cooling through the PRZ occurs on time-scales far shorter than the half-lives of radioactive parent elements, allowing the solution to assume a linear production of radiogenic daughter. One characteristic of the U-Pb rutile and titanite data produced in this study as well as two previous studies of lower crustal xenoliths (Davis et al. 2003; Schmitz et al. 2003) are discordant arrays of U-Pb dates. Measurements of varying grain size yield dispersion in measured U-Pb dates of hundreds of millions of years, defining a curvilinear array on a concordia diagram. This extreme discordance indicates a loss of equilibrium within the U-Pb system that could potentially be interpreted as the result of two different t-T paths: (1) reheating, violating the monotonic cooling history required to use Dodson's approach and (2) slow-cooling, which must consider radiogenic production over the hundreds of millions of years of potential PRZ residence. This requires that we utilize a solution to the diffusion-production equation that allows testing of both slow cooling and reheating time temperature paths, and that accounts for the production of specific Pb isotopes during prolonged residence within the PRZ.

Analytical solution to the diffusion equation

In the late 1950s and early 1960s as U-Pb zircon geochronology was being developed, volume diffusion theory and analytical solutions to the diffusion equation were derived in an effort to explain the loss of Pb and discordance observed in nearly all zircon measurements. Wetherill (1956) developed a graphical method using the concordia curve to determine both the timing of zircon crystallization and a secondary event, potentially a reheating event, that he hypothesized induced the diffusive loss of Pb,. The topology of data predicted by the episodic Pb-loss model is a straight line connecting the U/Pb ratios corresponding to the time of initial system closure (t_1) and the time of system reset or partial reset (t_2) (Fig. 1a). In this model the variation in U/Pb ratios along this discordia line is due to volume-diffusion's dependence on diffusion domain (a). The smallest domains are most susceptible to loss and yield the youngest dates, while the larger domains are less susceptible to Pb loss and yield older dates.

Seeking an alternative mechanism for Pb-loss within zircons, Tilton (1960), suggested a model for the 'continuous' loss of Pb within zircons. This diffusion model assumed that zircon grains were continually losing lead between the time of system formation until the time of system closure. Tilton (1960) presented an analytical solution to the diffusion equation for both U-Pb systems and thus plotted on a U-Pb concordia diagram. This analytical solution is restricted to using a constant diffusivity, i.e. temperature sensitive diffusivity cannot be modeled. Results from this solution are plotted in Fig. 1b (cross symbol). Start time in this sample calculation is 3,000 Ma. Unlike the secondary Pb-loss event model, the modeled data define a curvilinear array between the time of system formation and the origin. The curvilinear diffusion trajectory curves asymptomatically as it approaches the origin.

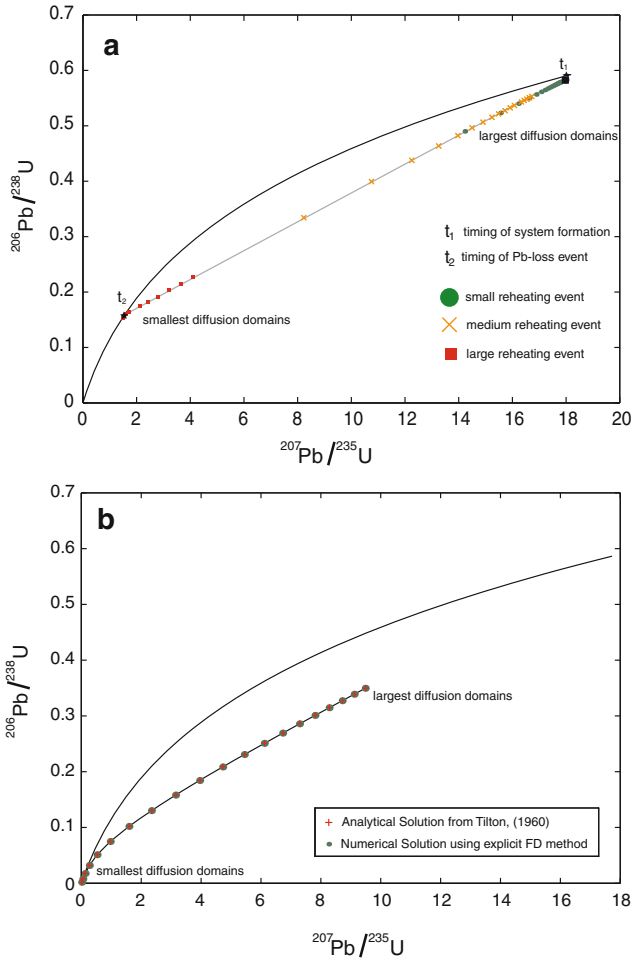

Fig. 1 Comparison of data topologies on U-Pb concordia diagram for **a** Episodic/reheating and **b** continuous or slow cooling time temperature paths. Forward calculated reheating time-temperature paths are plotted as symbols along with the graphical solution in *black* (*line*) from Wetherill (1956) **a** Discordant arrays of data are produced by rapidly cooling the sample at some initial time (t_1) followed by a secondary reheating event at t_2. The reheating event is modeled as a half-space model. Constant model parameters for all tested t-T paths include: grain sizes, start temperature and time, distance of sample from dike, diffusion kinetics, intrusion temperature and intrusion time. Only the size of the intrusion is varied. **b** A comparison between analytical (*crosses*) and numerical solution (*circles*) for continuous diffusion is used to test the accuracy of the finite difference solution

The asymptotic nature of the Pb diffusion trajectory as it approaches concordia is unique to continuous diffusion and will serve as a characteristic signature within real data sets.

Though the analytical solutions are restricted to a constant diffusivity, the difference in the data topology between the two models demonstrates how powerful the dual U-Pb system can be for monitoring time-variant Pb diffusion. The Wetherill and Tilton models for Pb loss are analogous to the end-member cases of reheating and slow cooling t-T paths, respectively. Below we will show how modeling reheating and slow cooling t-T paths within systems obeying temperature dependent diffusion will produce data topologies with the same distinguishable characteristics as the Wetherill and Tilton models.

Numerical solution to diffusion equation

A more flexible solution to Eq. 1 by finite difference methods can be used to calculate Pb concentration profiles for grains with variable temperature dependent diffusivity. A forward time, centered space solution to the diffusion equation provides a means to forward model synthetic U-Pb data for comparison to measured thermochronometric data (Schoene and Bowring 2007). In general terms, the concentration of radiogenic daughter is solved for by assuming a time-temperature path, parent element distribution, and grain size. Both age and grain size can be accurately measured for each real grain that is dated. The key parameter space that remains to be explored is the t-T path. In this exploratory study we assume a homogenous distribution of parent elements. By forward calculation of the Pb concentrations for a series of grain sizes, we can create a synthetic data set that includes the predicted Pb diffusion profile, grain size vs. age curve, and data topology in U-Pb concordia space, for any pre assumed t-T path. The correct time temperature path is qualitatively deduced by how synthetic data compare to measured thermochronometric dates. The accuracy of the finite-difference solution has been evaluated by comparing results (at a constant T) to the analytical solution developed by Tilton (1960). Figure 1b shows the results of a comparison of constant diffusivity between the finite difference (circles) and analytical solutions (cross). The U/Pb values produced by the numerical solution agree with no more than 0.4% deviation from the analytical solution.

Data topology

Resolving a unique cooling path

The nearly identical data produced by both slow cooling and reheating has long been noted and debated in thermochronology (Heizler 2002; Hodges and Bowring 1995; Schoene and Bowring 2007). In past studies, geological considerations and the magnitude of local and regional thermal events have been used to decide between slow-cooling and reheating t-T paths (Hodges and Bowring 1995). Ambiguity in a rock's cooling path arises from the possibility that data from internal diffusion profiles and grain size-age relationships may be produced from either slow-cooling or reheating time-temperature paths. The finite difference solution to the diffusion equation can be used to demonstrate how the dual decay scheme can be

employed to distinguish between continuous diffusion in a slow cooling system and Pb-loss during some secondary event. Figure 2 shows the modeled U-Pb results from both reheating and slow cooling time-temperature paths. The Pb diffusion profiles (Fig. 2a) and grain size-age relationships (Fig. 2b) produced by the two t-T paths (Fig. 2 inset) are nearly identical and are beyond resolution of any analytical technique. The same t-T paths shown in the Fig. 2 inset are used to produce U/Pb ratios for both the ^{238}U and ^{235}U decay schemes and are plotted in U-Pb concordia space

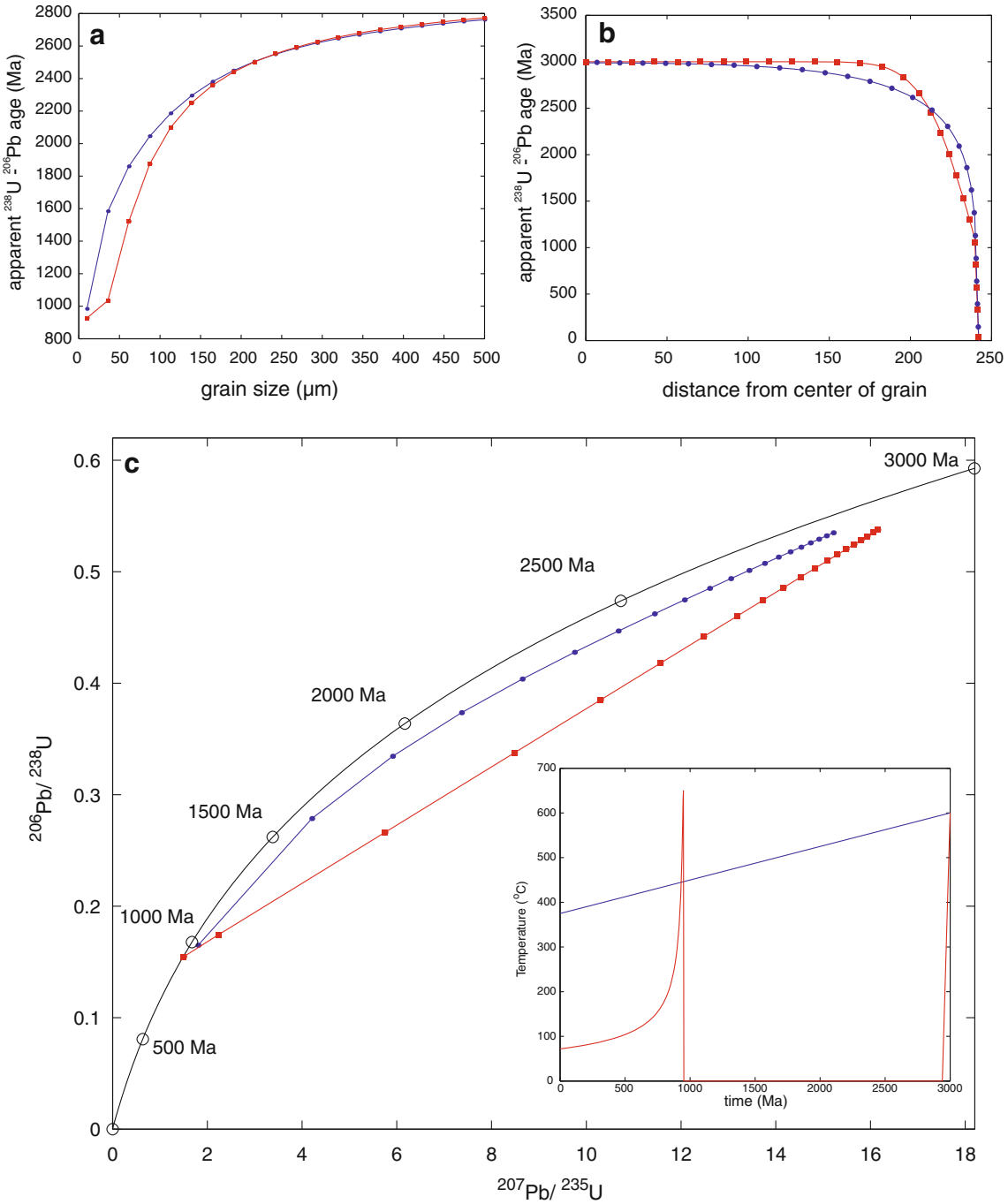

Fig. 2 Forward modeling of time temperature paths for reheating (*squares*) and slow cooling (*circles*) reveal the potentially indistinguishable data sets for both **a** grain size versus age relationships or **b** internal diffusion profiles; two data types often produced by single isotopic thermochronometric systems to elucidate t-T paths. Plotting U-Pb ratios for both systems on Concordia diagram **c** for the same reheating and slow cooling time temperature paths reveals data topologies that are distinguishable from one another. Diffusion occurring continuously during a slow cooling t-T path yields an asymptotic topology (*circles*) that is resolvable from the straight-line topology produced from the reheating t-T path (*squares*)

(Fig. 2c); the topologies are distinguishable for each t-T path. The slow-cooling modeled data define curvilinear arrays that become asymptotic near the lower intercept and are easily distinguishable from the straight-line of the reheating t-T path. The topology of data exhibited by a single sample will be an important tool to deciphering cooling paths for the case study region presented below. In the following sections we will explore why each t-T path results in the data topologies and how we can exploit these data trends to further interpret a samples t-T path.

Interpreting thermochronologic data on a concordia diagram also allows users to extract cooling rates from samples that do not exhibit perfect single domain behavior. In a grain size versus age plot (Fig. 2c), an internal fast diffusion pathway (grain cracks, defects or inter-growths) would yield a younger measured date and thus 'fall' off an array of data points. On a concordia diagram this data would still lie on the diffusion trajectory, however the data would have lower $^{206}Pb/^{238}U$ and $^{207}Pb/^{235}U$ ratios than well-behaved single domain grains of the same size. Mixing two separate diffusion domains that have experienced the same thermal history will always plot on the diffusion trajectory as a mixture between the domain sizes (Tilton 1960).

Slow cooling: relationship between internal Pb profiles and whole grain U-Pb dates

Diffusion is a length-scale dependent process. As such, radiogenic daughter that is produced within the cores of grains has a physically longer distance to travel than the daughter product produced at the edges. This results in a difference in the time of grain core versus rim closure. In the context of the slow cooling model the timing of entry and exit into the PRZ is recorded by the core and rims of a grain, respectively. If the sample cooled slowly enough, the resulting difference in time between core and rim closure may be significant, with longer durations in the PRZ yielding larger differences. To illustrate the relationship between a grain's internal Pb diffusion profile and whole grain U-Pb date, Fig. 3 shows a concordia diagram with the U-Pb ratios from along a grain's diffusion profile and the whole grain measurement that results from this internal profile. The internal U-Pb dates across the radius of this 200 micron grain (lower inset) were produced by a model run for slow cooling at a rate of 0.1°C/Ma (upper inset). Plotting the internal profile in 2 micron increments (circles) on a concordia reveals a curvilinear array spanning between the apparent time of core and rim closure. A whole-grain analysis (star) reflects mixing of these internal dates and their corresponding $^{238}U/^{235}U$ values, yielding a discordant analysis.

These profile U-Pb dates (dots) plotted in U-Pb concordia space however, are not concordant, because each U-Pb decay scheme has a unique PRZ as a result of different production rates for ^{206}Pb and ^{207}Pb. At high temperatures the diffusion of lead is the dominant process. As the rock cools and diffusion decreases, diffusion will come into balance with the high production rate ^{235}U-^{207}Pb system prior to the ^{238}U-^{206}Pb system (Fig. 3 upper inset). At the bottom of the partial retention zone, the production of ^{207}Pb will exceed the lower diffusivity that accompanies decreased temperatures, leading to the complete closure of the ^{235}U-^{207}Pb system prior to the ^{238}U-^{206}Pb system. This off-set in each U-Pb system's partial retention zone leads to a small excess of ^{207}Pb within slowly-cooled minerals as a direct result of the ^{235}U-^{207}Pb earlier system closure. We can see this effect of relative system closure by comparing the U-Pb system's internal age profiles (Fig. 3 lower inset) as well as the location of the internal U-Pb profile dates plotted on concordia.

The length scale dependency of diffusion also predicts that the resulting Pb diffusion profile and the temperatures of Pb retention will vary as a function of grain size, for any one time-temperature path. Because of this dependency, each individual grain size will have a distinct Pb diffusion profile, partial retention zone and whole-grain parent daughter ratio (i.e. location on concordia plot). Figure 4, serves to illustrate this relationship between these parameters. Lead diffusion profiles (Fig. 4a) are shown for grains with radii of 25, 50, 100 and 200 micrometers. Length scale dependency causes larger diffusion domains to retain Pb at higher temperatures than smaller grains. As stated above these apparent U-Pb dates across the radius of the crystal provide us with the approximate time-span of partial lead retention. Figure 4b shows how the timing of this partial lead retention can be superimposed on a slow cooling time-temperature path (0.1°C/Ma) for each grain size. The length-scale dependency of Pb, leads directly to a unique and separate PRZ for every grain size. As such, large and small grains can be used to resolve different parts of the time-temperature history. As an individual grain cools through its partial retention zone, the whole-grain age evolution through time of this grain can be tracked and plotted in U-Pb concordia space. The bulk grain age-evolution of 25, 50, 100 and 200 micron radius grains are plotted in Fig. 4c in 50 Ma increments. Each grain is concordant at the top of its PRZ when it first begins to retain Pb produced by a singular or narrow composition of $^{238}U/^{235}U$. As each grain cools through its' PRZ it retains Pb of different isotopic compositions as a result of the time-variant parent isotopic compositions ($^{238}U/^{235}U$). A whole-grain analysis of a grain with this internal diffusion profile will result in a mixture of these different Pb compositions that will become increasingly discordant as the grain incorporates a higher variability of $^{207}Pb/^{206}Pb$ (Fig. 4c). U-Pb whole grain dates for this same range of grain sizes and cooling

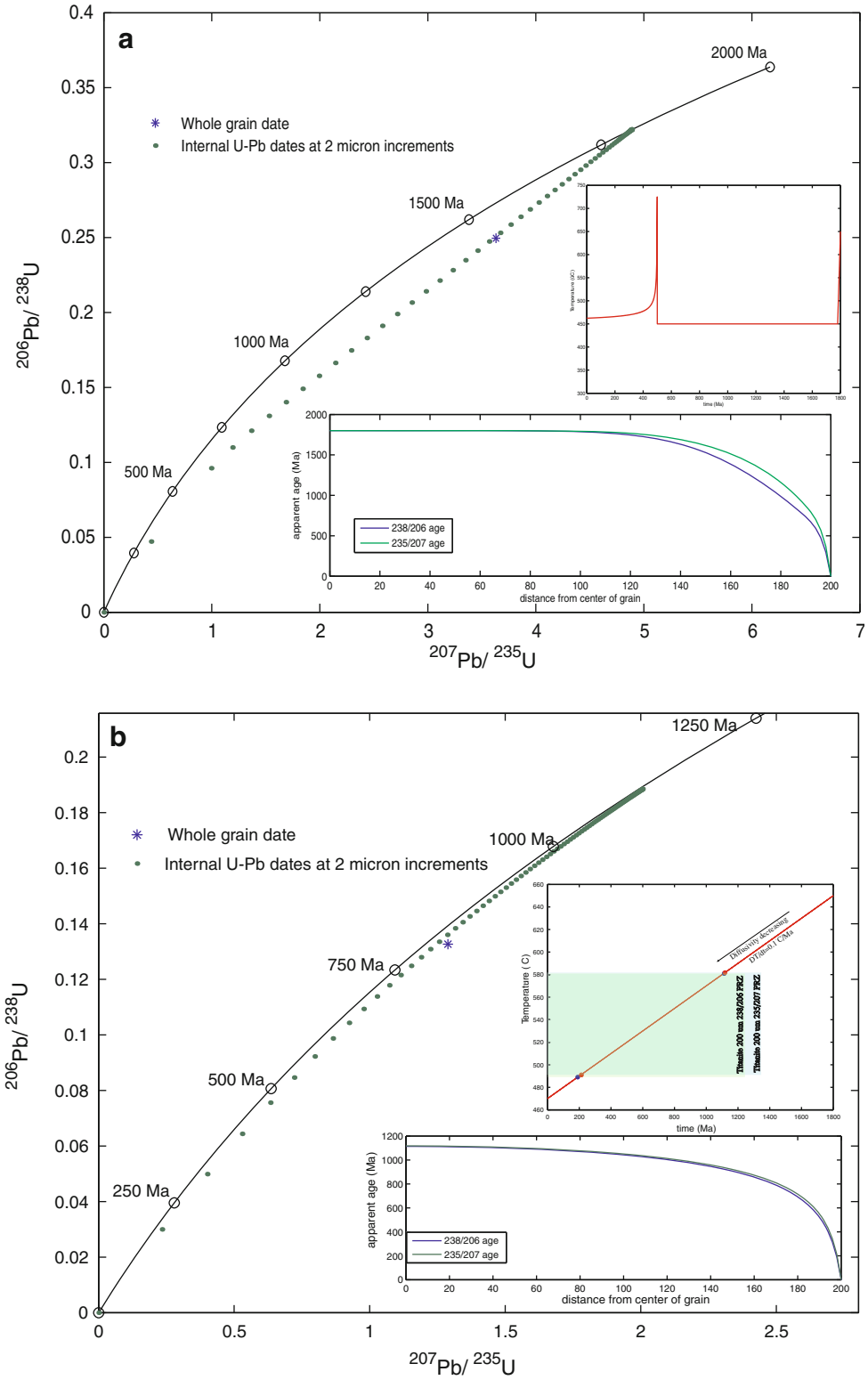

Fig. 3 Comparison of internal U-Pb profiles (*dots*) and whole-grain U-Pb dates (*star*) plotted on concordia diagram for **a** reheating and **b** slow cooling t-T paths. Slow cooling t-T paths **a** produce discordant whole-grain points as a result of mixing Pb produced from different isotopic compositions of U. Additional processes inducing disequilibrium between the different decay schemes are the offset between the ^{238}U-^{206}Pb and ^{235}U-^{207}Pb PRZ's (*upper inset*). The different decay rates for each daughter product leads to different times in which daughter production comes to balance with daughter diffusion. Reheating t-T paths **b** induce internal Pb diffusion profiles where the core records the initial time of cooling (t_1) and the grain rim, the subsequent reheating event (t_2)

paths is shown in Fig. 4d. The discordant array of data has an asymptotic topology that occurs as a result of each grain having its own unique PRZ and acquiring different amounts of variable isotopic compositions of Pb. Below we will see how these asymptotic trajectories in slow-cooling systems are highly sensitive to duration and thus cooling rate through the PRZ and can be used as a tool to determine time-temperature histories.

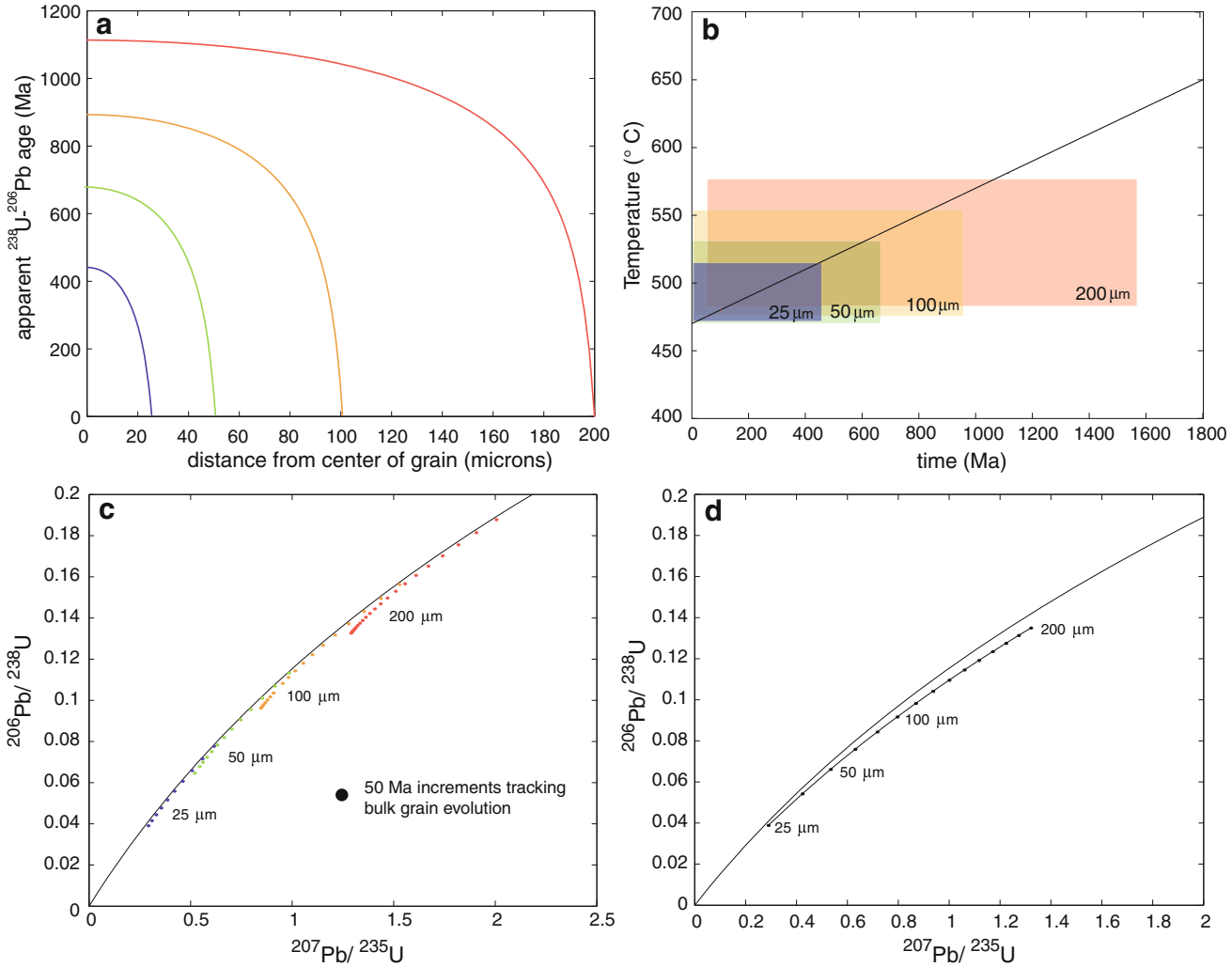

Fig. 4 For a single slow cooling path, variable grain sizes yield different ranges of internal U-Pb dates (**a**) with large grains retaining Pb at earlier times and higher temperatures. Subplot (**b**) plots the PRZ for each grain size on the tested time-temperature path. Each grain is recording a discrete region of the time temperature path. This results in a unique set of: internal U-Pb dates (**a**), and a different U-Pb whole grain date. Subplot (**c**) tracks several grains in 50 Ma increments. Upon entry into the PRZ every grain is concordant, meaning it contains Pb produced by a uniform $^{238}U/^{235}U$. Each grain becomes more discordant through time, as the whole grain begins to retain more Pb produced by the decay of different $^{238}U/^{235}U$. Length scale dependency of diffusion leads to discrete ranges of Pb retention for each grain size which in turn leads to the asymptotic topology (**d**)

Slow cooling: resolving unique cooling rates

Cooling rate estimates are derived from the relationship between cooling rate and duration in the PRZ; the slower the cooling rate through the PRZ the longer the duration. Forward modeled U-Pb data with variable linear cooling paths are plotted in Fig. 5. Results of calculations using titanite (Cherniak 1993), rutile (Cherniak 2000) and apatite (Cherniak et al. 1991) diffusion kinetics are plotted in Figs. 5 a, b and c respectively. For each set of kinetics, cooling rates between 10 and 0.075°C/Ma are explored. For cooling rates of 10°C/Ma or faster, data plots near the model start time (3,000 Ma). This relatively rapid cooling rate through the PRZ causes little to no difference between large and small grains. For cooling rates slower than 10°C/Ma the effect of grain size causes a dispersion of data along concordia, with smaller grains yielding younger dates. Cooling rates slower than ~0.25°C/Ma are not only dispersed according to grain sizes but become discordant and highly asymptotic to concordia. A general trend of slower cooling rates and thus longer time spent within the PRZ, is shown to yield extended arrays of data. Calculated data sets for multiple minerals with different diffusion kinetics are shown to demonstrate the relative independence between diffusion kinetics and data topology. Though each mineral retains Pb at a different temperature range (Fig. 5 insets), the data topologies for all three minerals at one cooling rate are similar. Trends between data topology and cooling rate

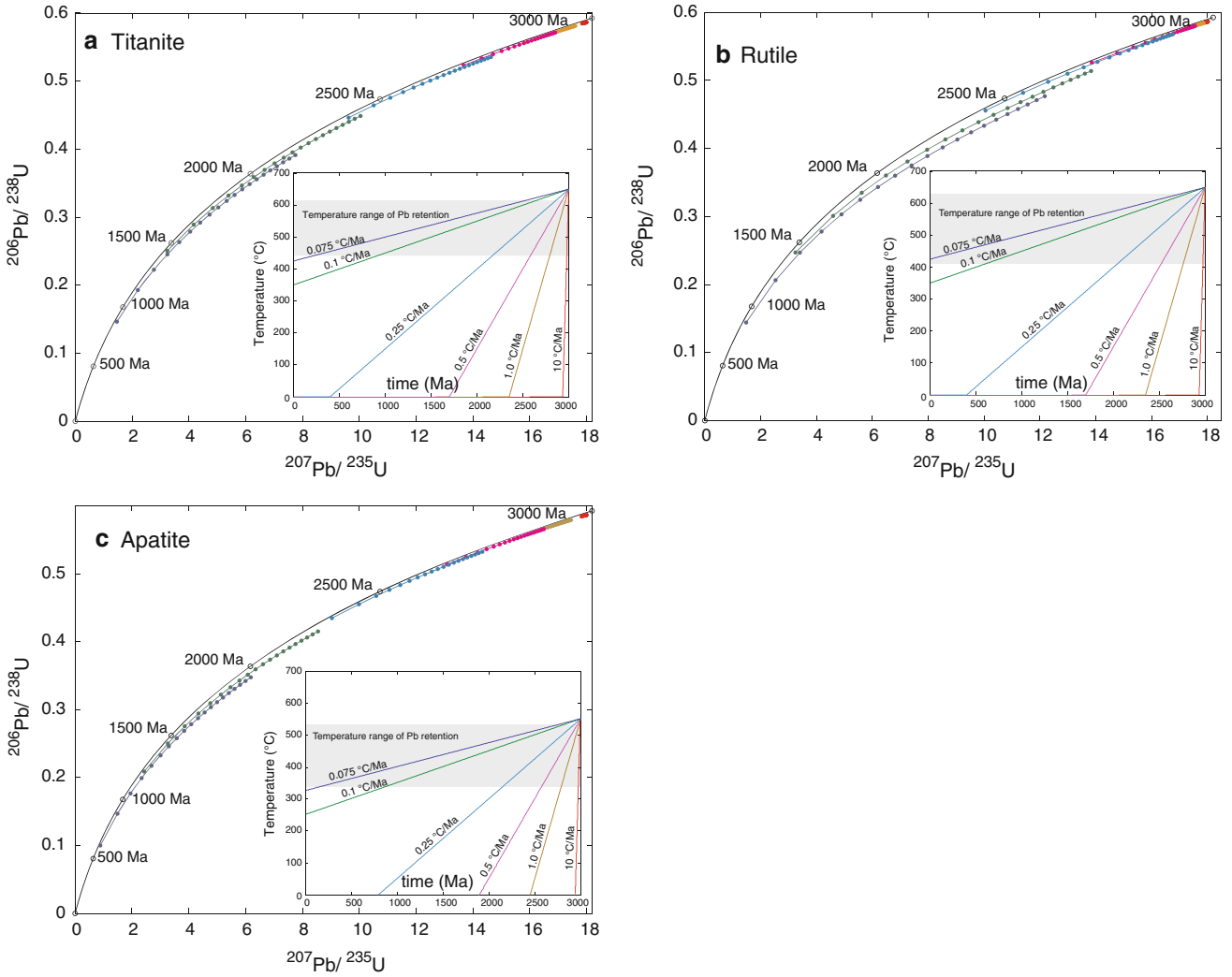

Fig. 5 Series of concordia plots showing the results of slow cooling time-temperature paths at a variable cooling rate. Colors of data correlate to the colors of cooling rates shown in the inset time-temperature path. Slower cooling rates yield longer durations in the PRZ, in turn resulting in longer discordant data arrays. Start time and temperature, grain sizes are kept constant. Only the cooling rate and diffusion kinetics are variable; **a** titanite, **b** rutile, **c** apatite. Modeled results using multiple diffusion kinetics are plotted to demonstrate the potential for different U-Pb thermochronometers as well the relative independence between diffusion kinetics and data topology

will not only aid in deciphering cooling rates, but also help us resolve time-temperature paths even for minerals such as rutile where the temperature of Pb-closure is still debated.

Episodic Pb-loss and reheating t-T paths

Episodic Pb-loss or reheating can induce discordant U-Pb data similar to what is observed in accessory minerals from lower crustal xenoliths. In this end member thermal history, a rock has experienced rapid cooling during some initial event followed by open to partially open system behavior during a subsequent reheating event. As shown in Fig. 1a, the upper intercept records the initial time of system closure, while the lower intercept records the time of a secondary reheating event.

As in the case of slow cooling, each whole grain analysis is discordant a result of mixing an internal Pb diffusion profile of different U-Pb ratios. Figure 3b shows a plot of the calculated U-Pb dates along the radius of a 200 um grain on a concordia diagram (dots). The model whole grain date that results from this profile is also plotted (star) and unlike the case of slow cooling, lies *on* the mixing line between the initial rapid cooling (t_1) and subsequent reheating event (t_2). Prior to the reheating event, this grain had a uniform profile across the radius. The heating event results in a continuous gradient of dates along the radius of the grain that lie between the initial and secondary event.

The finite difference diffusion model allows us to explore the effects of different heating magnitudes and durations. Figure 1 shows the results of forward modeled titanite U-Pb dates for reheating of grains of varying size. A reheating event at 1,000 Ma is modeled as a dike or half-space intrusion of variable half-widths and an initial temperature of 1,200°C. All parameters, including start time and temperature, distance from the intrusion to the sample, grain sizes and initial cooling rate are held constant. Only the size of the intrusion is varied between model runs. Comparison of reheating data sets to the linear cooling reveal that heating events such as the 100 m half-width dike cause sufficient lead loss to completely change the data topology. Much like the internal profile for a reheating path shown in Fig. 3b, the variable grain size data define a linear array between the initial start of the system and the time of reheating (Fig. 1b). Small deviations from the linear array are due to the conductive cooling of the half-space after reheating. Larger intrusions on the order of 1 km, yield extremely discordant data arrays that nearly span the distance between primary and secondary events. A large event will induce almost complete Pb loss, with modeled data clustered at a lower intercept. For a given mineral, there is a trade-off between duration and temperature of heating events such that small intrusions of high temperature can induce the same Pb loss as larger intrusions at lower temperatures. Analysis of multiple thermochronometers can solve this ambiguity and deliver a unique cooling path (Schoene and Bowring 2007).

Multiple sample approach

In addition to using the topology of individual data sets to determine cooling path and rate, we can employ a multiple sample approach where data from multiple xenoliths, each of a different depth, contribute to a unique thermal history for the entire lithospheric column. This method assumes that the thermal history recorded by a suite of xenoliths reflects that of the lithosphere. Let us consider the two end-member t-T paths of reheating and slow cooling within a section of lithosphere where three xenoliths, each from a different depth are dated.

Slow cooling t-T paths for samples of variable depth can be modeled by allowing a column of lithosphere at a specified initial temperature, thickness and internal heat production, to cool by conduction. The purpose of this thermal model is to predict how variable depths influence the time temperature path and the resulting U-Pb thermochronometric data. Time-temperature paths for 'samples' at 20, 30 and 40 km depths within the lithosphere have the same shape, cool at comparable rates, but at different times (Fig. 6a). The initial cooling along an exponential t-T path is controlled by sample depth, with the shallowest samples cooling fastest and the deep sample the slowest. Once a near steady thermal state is reached, however, samples cool at similar rates independent of residence depth (Fig. 6a inset). Like modeled data from previous slow cooling model runs, modeled U-Pb data arrays are highly discordant and become asymptotic to concordia. Because the

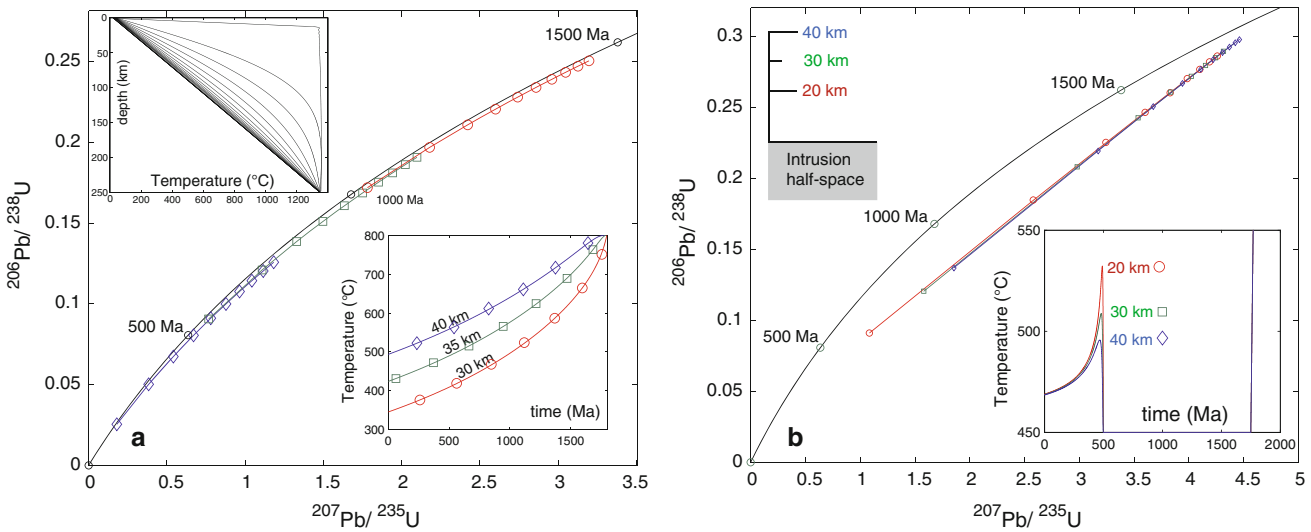

Fig. 6 Forward modeling U-Pb data for multiple xenolith samples of different depths within the lithosphere produced by thermal models for lithosphere **a** slow cooling and **b** reheating. Multiple sample analyses of a Slow cooling **b** lithosphere yields curvilinear discordant arrays of U-Pb data with resolvable and unique upper and lower intercepts. Reheated lithosphere (**a**) produce overlapping *straight lines* of discordant U-Pb data with a common irresolvable lower intercept. The intercepts of these *lines* are coincident in with the timing of initial cooling and the reheating event or with cooling shortly after

time of entry and exit into the PRZ is different for each depth, both the lower and upper intercepts of these data arrays are *resolvable* from one another.

A similar multiple sample analog can be set up to examine the effects of reheating on a column of lithosphere where 3 xenolith samples, each at a different depth, are heated during a large-scale regional thermal event. The duration and temperature of reheating events required to induce a similar magnitude of discordance as those observed in the data are considerable (>50% fractional loss Pb); requiring holding times on the order of millions of years for reheating events below 1,000°C and durations in the hundreds to thousands of years at mantle temperatures (Schmitz et al. 2003). Any significant thermal event such as this will likely be recorded by each sample within the lithosphere with the effects of the reheating event varying as function of the sample distance from the heat source. To simulate this setting, a half-space model was used to heat the base of the lithosphere, with samples positioned at 20, 30 and 40 km from the heat source margin (Fig. 6b inset). Because each sample is from a different distance from the source of heat, each will experience a different magnitude of reheating, simulating the effects of variable xenolith residence depth. The U-Pb thermochronologic data that results from t-T paths for each sample are plotted on concordia diagram in Fig. 6b. Unlike the slow cooling end member, the discordant arrays of data *share a common* lower intercept that is coincident in time with the reheating event.

Testing the effects of magmatic exhumation

In addition to understanding the thermal history of lower crustal samples, we must quantify the thermal affects of volcanic exhumation on the U-Pb systematics in accessory phases. Petrologic and experimental studies of xenolith bearing magmas (Canil and Fedortchouk 1999; Edgar et al. 1988; Eggler and Wendlandt 1979; Esperanca and Holloway 1987) along with dynamical force balancing (Morin and Corriveau 1996; Sparks et al. 2006; Spera 1984) allow us to estimate the temperatures and holding times experienced by a lower crustal sample during exhumation. These conditions can then be used to calculate the minimum temperatures and holding times required to perturb U-Pb systematics within accessory phases.

Reliable estimates of xenolith residence time and host magma temperature are key to understanding the effects of volcanic exhumation on U-Pb systematics. Magma ascent rates for alkalic, mantle-derived magmas can in general be considered a rapid process. The occasional presence of diamonds, abundant xenoliths, some as large as 100 cm in diameter, imply that eruption rates are fast enough to transport the xenolith load from lower crustal and upper mantle depths. Typical ascent rates for alkaline magmas are estimated to be on the order of 10^1–10^3 cm/s or 1–5 day durations from upper mantle to lower crustal depths (Rutherford 2008). Kimberlite and minette eruption rates have been further refined to rates on the order of hours to days by both dynamic calculations and experimental studies (Canil and Fedortchouk 1999; Morin and Corriveau 1996; Rutherford 2008). An upper bound of magma temperatures can be provided from estimates of magma liquidus temperatures, which for kimberlite and minette magmas has been estimated between 1,050 and 1,200°C (Edgar et al. 1988; Eggler and Wendlandt 1979; Esperanca and Holloway 1987). The actual magma transport temperatures are likely lower than the liquidus temperatures as a result of heat loss to country rock/xenoliths and volatile degassing (Sparks et al. 2006).

The extreme upper boundary conditions of 5 days and 1,200°C can be used to estimate the maximum effects of volcanic transport on the topology of U-Pb data. This calculation has typically been solved for using the fractional loss equations from Crank (1956). This calculation provides us only with a minimum estimate to the conditions required to induce Pb-loss, as the solution assumes a homogenous initial distribution of diffusant within the crystal prior to perturbation. Accessory minerals that have experienced slow cooling or reheating, however, have pre-existing rounded diffusion profiles that will respond more slowly to diffusive loss during thermal perturbation. In reality the transporting magma would have to be hotter and/or heat longer to induce the same amount of fractional loss as with a homogenous distribution of Pb. The finite different model presented above can be used to simulate the conditions of magmatic heating on a rounded diffusion profile demonstrating that the fractional loss of Pb is as much as 10% less with a rounded initial profile when compared to a homogenous one. The finite difference calculation suggests that short-lived high temperature heating events of this magnitude do induce some Pb-loss even on grains with rounded initial profiles. Figure 7 shows the predicted effect of magmatic heating on U-Pb thermochronologic data. The 5 day maximum of holding time at the temperature of 1,200°C is shown to have a slight effect on the topology of U-Pb data, shifting all data points to lower U/Pb values. The loss of Pb, however, has little effect on the topology of U-Pb data and the final interpretation of a t-T path. This observation coupled with the likelihood that the eruptions of the xenolith bearing lavas are likely faster and cooler than the maximum limit modeled here, suggest that the effect of Pb loss from magmatic heating can largely be ignored. Only titanite and apatite kinetics allow loss of Pb, there is no appreciable Pb loss (<0.25%) using rutile diffusion kinetics. The accuracy of this finite difference calculation can be tested using a homogenous initial concentration of Pb prior to the

reheating event and comparing the results to the fractional loss equations calculated with the same initial conditions (Fig. 7 inset).

Rutile diffusion kinetics

Calculating Dodson closure temperatures from experimentally determined diffusion kinetics for Pb in accessory phases provides a means to compare the relative closure between different phases. The Dodson closure temperatures (T_C) calculated using kinetic values from Cherniak and Watston (2001), Cherniak (1993, 2000) and Cherniak et al. (1991) yield a relative order of Pb closure: Zircon ($T_C > 1{,}000$°C), Rutile ($T_C \sim 600$–700°C), Titanite ($T_C \sim 600$–650°C) and Apatite ($T_C \sim 450$–500°C) (Fig. 8). Empirical estimates for the temperatures of Pb closure yield a relative order that contrasts with experimentally determined values: zircon and Monazite ($T_C > 1{,}000$°C) Titanite ($T_C \sim 600$–650°C), Apatite ($T_C \sim 500$–550°C), Rutile (T_C 450 ± 50°C) (Mezger et al. 1989; Schmitz et al. 2003). The rutile Pb closure temperature estimates from over ten U-Pb thermochronologic studies have been compiled and plotted in Fig. 8 (black circles). Estimates of rutile closure, grain size and cooling rate are cited directly from the reference when available. When closure estimates were unspecified, comparison between available titanite and apatite U-Pb and amphibole, phlogopite, muscovite $^{40}Ar/^{39}Ar$ data were used to bracket a temperature. In all but one study, rutile U-Pb dates are younger than titanite U-Pb and amphibole $^{40}Ar/^{39}Ar$ dates. The exception to this is an overlapping rutile U-Pb and amphibole $^{40}Ar/^{39}Ar$ dates from a moderately slowly cooled terrane ($dT/dt = 1.5$°C/) (Mezger et al. 1989). In four studies, rutile U-Pb dates are younger or overlap with apatite U-Pb dates (Corfu and Easton 2001; Corfu and Stone 1998; Flowers et al. 2006; Schmitz et al. 2003b). In several additional studies, rutile Pb closure is constrained between Titanite U-Pb/Amphibole $^{40}Ar/^{39}Ar$ and the lower temperature muscovite and biotite $^{40}Ar/^{39}Ar$ chronometers, (Anderson et al. 2001; Flowers et al. 2006; Mezger et al. 1989; Miller et al. 1996; Moller et al. 2000). Two conclusions can be drawn from this data compilation (Fig. 8): (1) Empirical estimates of rutile closure are significantly lower than

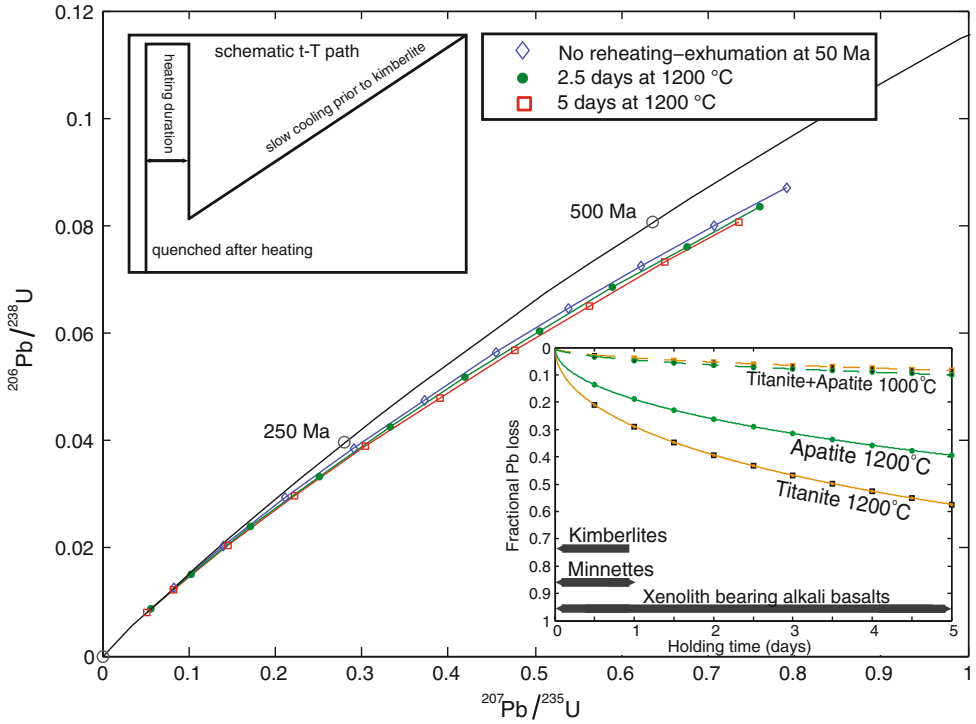

Fig. 7 Concordia plot showing the effects of magmatic exhumation on U-Pb data. Finite difference model tests the effects of short-lived heating events on thermchronometers with rounded initial profiles. Rounded diffusion profiles lessen the diffusant loss during a secondary reheating event. Independent constraints on magma temperature and eruption rate can only place maximum heating conditions at 1,200°C and 5 days, though lower temperatures and shorter holding times are more likely. Decreasing the magma holding temperature to 1,000°C yields Pb loss below 1%. Titanite and apatite kinetics are used, rutile kinetics predict negligible loss at these conditions. Figure inset show an accuracy test of this calculation using the same initial conditions in the numerical solution (*blocks and circles*) as those used by the analytical solution (*solid lines*)

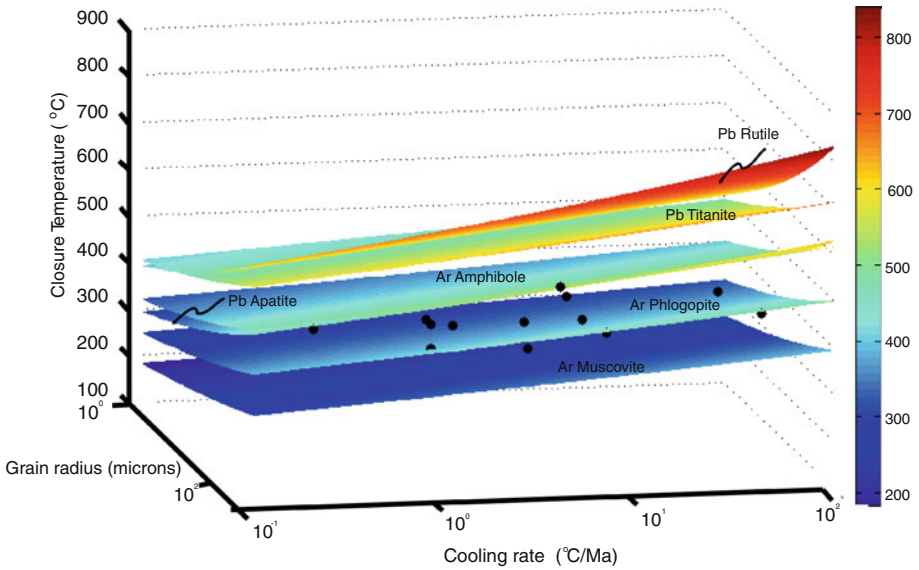

Fig. 8 Three-dimensional plot showing the variation of Dodson closure temperature as a function of both cooling rate (°C/My) and grain radius (μm). Three-dimensional planes are calculated using Dodson equations and experimentally measured diffusion kinetics. *Circles* mark the estimated closure for rutile based on empirical studies, see text for references. Diffusion kinetics for $^{40}Ar/^{39}Ar$ chronometers are from Harrison (1982), Giletti (1974), and Hames and Bowring (1994)

predicted by diffusion kinetics, (2) Rutile has a Pb closure temperature between 400 and 500°C.

Case study

Geologic overview

Eocene minettes and kimberlites (~50 Ma) have exhumed a large population of lower crustal xenoliths just east of the Cordilleran deformation front in central Montana. Beneath the Phanerozoic sedimentary cover, the Archean Medicine Hat Block (MHB) to the north and the Wyoming Province (WP) to the south are separated by the largely unexposed Great Falls Tectonic Zone (GFTZ) (Davis and Ross 1999; Gorman et al. 2002; Mueller et al. 2005; Mueller et al. 2002). To demonstrate the numerical and laboratory techniques described here, a case study for lower crustal xenoliths collected from the Sweetgrass Hills minette within the MHB are presented. U-Pb zircon data from basement rocks sampled by drilling reveal crystallization ages that range from 2.6 to 3.2 Ga, with the majority of samples yielding ages of ~2.7 Ga (Villeneuve et al. 1993). The Deep Probe seismic refraction study conducted as part of Lithoprobe, produced a high-resolution model for crust beneath the Northern Rockies (Gorman et al. 2002). Velocity models indicate a thick (10–15 km) high velocity layer beneath the region at depths between 40 and 55 km. Previous zircon U-Pb analyses from lower crustal xenoliths exhumed from the MHB yield a range of dates between 2.7 and 1.7 Ga (Davis et al. 1995). While tonalitic middle to lower crustal xenoliths from the Medicine Hat Block indicate Archean zircon growth, all lower crustal xenoliths analyzed by these workers (four mafic and one felsic sample) yielded only ~1.8–1.7 Ga zircon dates. This led to an interpretation that the high-velocity layer is a Paleoprotoerzoic magmatic under-plate associated with the formation of the GFTZ (Gorman et al. 2002).

Methods

Sample description and petrology

Three xenoliths from the Sweet Grass Hills minettes were selected for analysis. Two of the samples (05SG02 and 05SG05) have similar primary metamorphic mineral assemblages of Grt + Pl + Kfs + Bt (minor) ± Sil + Qz + Rt (Whitney and Evans 2010). The third sample contains the mafic assemblage Grt + Cpx + Pl + Rt + Ilm. All three samples are well-preserved and exhibit granoblastic textures. Sample 05SG05 contains mm-scale gneissic layering defined primarily by garnet, feldspar, and quartz. In all samples, rutile is relatively abundant (~0.3–0.6 volume %–see appendix for details), occurs in the matrix and as inclusions within garnet and other major phases, and is interpreted as part of the peak metamorphic assemblage. This is an important constraint because it establishes initial rutile growth prior to or during development of peak temperatures, which are well above the temperatures of rutile Pb retention (Fig. 8). Thus, the mineral can be utilized as a reliable thermochronometer. Minor ilmenite overgrowths on some rutile grains represent a late phase that probably developed during exhumation.

Thermobarometric estimates of peak metamorphic conditions were determined via several methods. First, initially determinations used the program TWQ 2.34 (Berman 1991, 2007). Isochemical phase diagrams were

also calculated with the program Perple_X (Connolly and Petrini 2002) using the Na_2O-CaO-K_2O-FeO-MgO-Al_2O_3-SiO_2-H_2O-TiO_2 chemical system. Temperatures were also estimated based on Zr-in-rutile thermometry (Ferry and Watson 2007; Watson et al. 2006). The best estimates of peak metamorphic conditions for samples 05SG02, 05SG05 and 05SG20 are 0.8 GPa/900°C, 1.1 GPa/900°C and 1.3GPa/890°C, respectively. These data allow us to construct a relative stratigraphy between the MHB samples; from shallow to deep, 05SG02, 05SG05 and 05SG20. Thermobarometry data is included in the inset of Fig. 9. Additional sample description and details of thermobarometric calculations are included in the appendix.

U-Pb laboratory methods

Accessory phases used by this study were extracted from collected xenoliths following standard rock crushing and mineral separation procedures. Crushed rocks were then hand washed, dried and separated using standard magnetic and heavy mineral separation techniques were used to isolate heavy minerals such as apatite, titanite, rutile and zircon. Prior to dissolution and analysis, all grains were photographed and measured. In the case study presented here, rutile was dated by U-Pb methods following procedures outlined by Schmitz et al. (2003) and Schoene and Bowring (2007). A mixed ^{205}Pb-^{233}U-^{235}U tracer solution was used for all ID-TIMS analyses. Samples were dissolved using standard Parr vessel HF/HCl treatments. Separates of U and Pb are purified separately using standard HBr and HCl column chemistry. Typical Pb blanks ranged between 0.5 and 1.2 pg. All U and Pb analyses were run on the Sector 54 Thermal Ionization Mass Spectrometer (TIMS) at MIT.

For sample presented here, at least ten rutile grains of varying size were dated by the above methods. The typical grain sizes (shortest radius) in lower crustal samples range between 10 and 250 microns. Grains without inclusions that had euhedral habit and no cracks produced reproducible grain-size age relationships. In preliminary study, poor quality grains, in particular large non-gem quality black rutiles often displayed multi-domain behavior, yielding younger U-Pb dates than previous analyses from a much smaller grain. To empirically demonstrate the presence of diffusion profiles, the edges of grains were isolated for U-Pb analysis. Whole rutile grains from sample 05SG05 were mounted in epoxy resin with the *a/b* axis of grains exposed at the polishing surface. Grains were then polished to remove over 95% of material. Isolated rims were dated using the procedures described above. Rutile grains from sample 05SG02 were mechanically abraded in attempt to enhance the older recorded cooling history within the core of the grain. Both grain cores and rims were excluded from comparison to forward difference models, which calculate data for whole grains.

Zircon grains from lower crustal rocks often have complicated growth histories, with individual grains

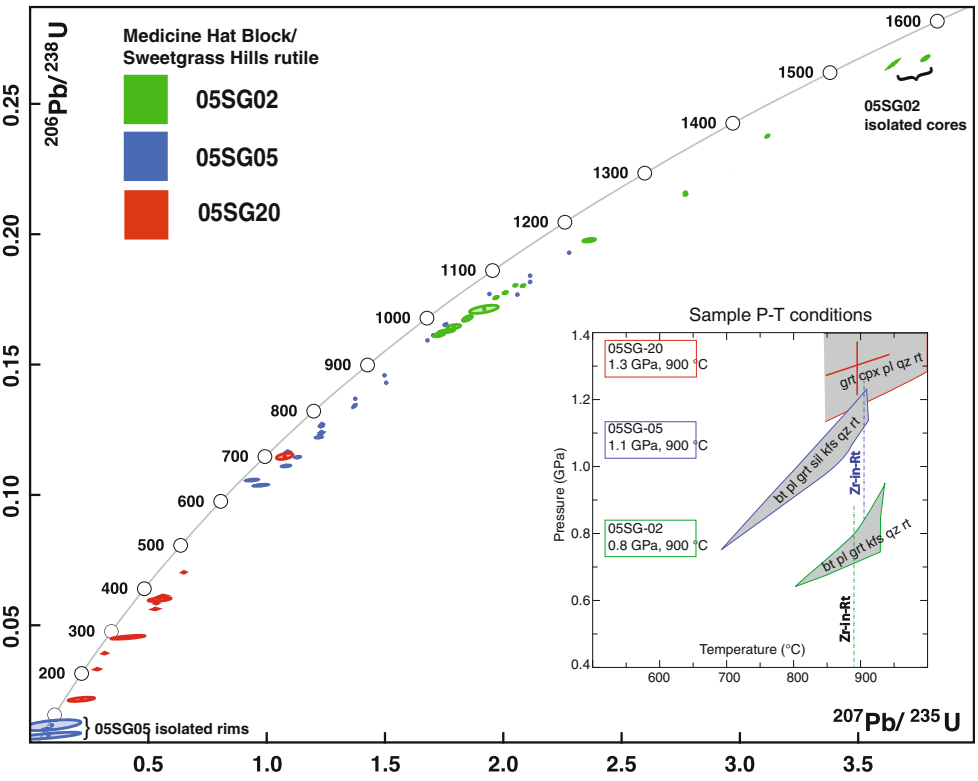

Fig. 9 Rutile U-Pb data plotted on a single Concordia diagram. Samples 05SG02(green), 05SG05(*blue*), and 05SG20 (*red*). Figure inset shows P-T diagram of thermobarometry, where the shaded regions represent calculated stability fields for the peak assemblages from phase assemblage diagrams. Solid red lines for 05SG20 show intersection of Grt-Cpx-Pl-Qz equilibria calculated with TWQ. Dashed lines are Zr-in-rutile thermometer results. See appendix for more detailed description

consisting of an older core surrounded by as many as 1–3 periods of zircon growth. Procedures for dating complex zircons include imaging grains by Cathode Luminescence (CL) followed by micro-sampling each distinct zircon growth history for analysis using Chemical Abrasion U-Pb Thermal Ionization Mass Spectrometry (CA-TIMS) (Mattinson 2005).

Results

U-Pb data

Zircons were recovered only from samples 05SG02 and 05SG05, the middle/lower crustal felsic granulites. and analytical results are tabulated in Table 1. Grains from sample 05SG05 were homogenous and yielded dates of ~1.8 Ga. Distinct cores of grains from 05SG02 were as old as 2.7 Ga, with rims plotting discordantly between ~2.7 and 2.0 Ga. Whole grain analyses from 05SG02 were discordant between 2.7 and 2.0 Ga. There were no zircons recovered from sample 05SG20.

Single grain rutile analyses of variable grain sizes (Fig. 9) define discordant data arrays for all three samples. The most shallow sample from the MHB, 05SG02, yields ^{238}U-^{206}Pb dates that range between ~ 1,000 and 1,400 Ma, sample 05SG05 a range between ~600 and 1,100 Ma and the deepest sample 05SG20 a range between ~200 and 400 Ma. Each array of data define a curvilinear trajectory that becomes asymptotic to concordia. The data as a whole, roughly define a single trajectory, with the oldest analyses from sample 05SG20 overlapping in concordia space with a young analyses from 05SG05. The same phenomena occur between several old analyses from 05SG05 and younger grains from 05SG02.

Mechanically isolated rutile rims from sample 05SG05 yield overlapping ^{238}U-^{206}Pb dates within error of the minette host rock eruption age and demonstrate empirically that volume diffusion is operating in these grains. Isolated grain cores from sample 05SG02 yield U-Pb dates far older than whole grain, again empirically demonstrating the presence of diffusion profiles. Euhedral, gem quality rutile grains in samples 05SG02 and 05SG05 often contained no common lead, with analyses yielding laboratory blank levels. High common Pb rutile grains typically have black ilmenite rims and ilmenite intergrowth within the interior of grains. Sample 05SG05 had no ilmenite intergrowths and demonstrated a near perfect age versus grain size relationship, with the smallest grains yielding the youngest dates and the largest yielding the oldest. Sample 05SG02 behaved similarly at small grain sizes, between 20 and 50 microns, however this relationship breaks down with larger poor quality grains that contained ilmenite intergrowths. Rutile U-Pb results are tabulated in Table 2.

Modeling U-Pb data

Here we evaluate the potential time-temperature paths that can explain the U-Pb data presented above. Each sample is considered individually and fit with modeled data from both reheating and slow-cooling T-t paths. Modeled grain sizes for each sample use the minimum and maximum

Table 1 Zircon U-Pb data

Fractions	206Pb/238U	±2σ %	207Pb/235U	±2σ %	207Pb/206Pb	±2σ %	Age (Ma)[a]			Corr. coef.	Pbc (pg)	Pb*/Pbc
							206Pb/238U	207Pb/235U	207Pb/206Pb			
05SG02:zircon												
z1.1	0.5055	0.09	13.0900	0.11	0.1878	0.06	2637	2,686	2,723	0.839	4.92	72
z2	0.5212	0.07	13.7830	0.09	0.1918	0.06	2704	2,735	2758	0.788	1.35	155
z3	0.5097	0.07	13.2320	0.09	0.1883	0.05	2,655	2,696	2,727	0.823	1.95	415
z4	0.3699	0.17	6.7110	0.20	0.1316	0.09	2,029	2,074	2,119	0.881	0.80	66
z5	0.4297	0.06	9.2243	0.08	0.1557	0.05	2,305	2,361	2,409	0.763	0.75	121
z6	0.4307	0.14	9.3750	0.18	0.1579	0.10	2,309	2,375	2,433	0.810	1.22	87
z7	0.4779	0.54	12.0430	0.57	0.1828	0.17	2518	2,608	2,678	0.952	1.85	26
z9	0.5018	0.06	13.0260	0.08	0.1883	0.06	2,621	2,682	2,727	0.699	0.74	250
SG05:zircon												
z3	0.3238	0.10	4.9730	0.26	0.1114	0.22	1,808	1,815	1,822	0.601	0.84	1,013
z2	0.3242	0.06	4.9556	0.10	0.1109	0.06	1,810	1,812	1,814	0.854	1.12	247
z4	0.3260	0.16	5.0510	0.70	0.1124	0.61	1,819	1,828	1,838	0.660	39.25	7

Pb* Radiogenic lead

[a] Isotopic dates calculated using the decay constants $\lambda 238 = 1.55125E-10$ and $\lambda 235 = 9.8485E-10$ (Jaffey et al. 1971)

Table 2 Rutile U-Pb data

Fractions	Grain descr.	Grain size (μm) Concentration (ppm)				206Pb/ 238U	% err	207Pb/ 235U	% err	Age (Ma)			Corr. coef.	Common est. Pb		
		w	l	U	Pb*					206 Pb/ 238 U	207 Pb/ 235 U	207 Pb/ 206 Pb		Pb (pg)	Blank (pg)	Pb*/ Pbc
05SG02 rutile																
r09-1	1	25	150	38.1	5.5	0.1645	0.5390	1.7908	1.6059	981.6	1042.1	1171.4	0.46	1.84	0.60	1.00
r09-2	1	30	185	71.1	11.6	0.1757	0.2731	1.9692	0.5024	1,043.2	1105.0	1,228.8	0.63	0.80	0.80	8.11
r09-3	1	50	140	40.7	6.7	0.1776	0.2447	2.0082	0.4707	1,053.7	1,118.3	1,246.1	0.58	0.53	0.52	15.33
r09-4	1	50	150	110.7	20.1	0.1977	0.3483	2.3629	1.1357	1,162.9	1,231.5	1,353.6	0.46	7.66	0.60	3.52
r09-5	1	60	170	63.0	10.6	0.1804	0.1704	2.0510	0.3748	1,069.1	1,132.6	1,256.4	0.50	0.79	0.78	26.91
r09-6	1	25	130	103.6	16.3	0.1712	0.9136	1.9182	3.1668	1,018.6	1,087.5	1,228.0	0.59	2.13	2.00	2.09
r09-7	1	25	140	65.9	9.9	0.1628	0.3866	1.7596	1.9052	972.4	1,030.7	1,156.5	0.54	0.77	0.77	3.85
r09-9	1	18	140	244.7	36.4	0.1615	0.5047	1.7293	1.3400	965.4	1,019.5	1,137.6	0.54	0.96	0.96	5.75
r09-12	1	60	95	39.5	6.1	0.1677	0.6696	1.8483	1.1352	999.4	1,062.8	1,195.4	0.67	0.90	0.89	7.55
r1	2	220	500	49.7	11.2	0.2376	0.1936	3.1162	0.2253	1,374.0	1,436.7	1,530.9	0.86	5.71	1.30	157.78
r3	2	100	400	107.2	21.6	0.2152	0.1510	2.7709	0.2258	1,256.5	1,347.7	1,495.6	0.68	6.62	1.50	32.79
r5	2	100	225	13.8	2.3	0.1803	0.2030	2.0832	0.3792	1,068.6	1,143.3	1,287.9	0.67	3.29	1.50	7.09
r6	2	75	245	78.1	15.8	0.2159	0.1077	2.7684	0.1804	1,260.4	1,347.1	1,487.5	0.64	2.30	1.50	31.71
r10	A,2	–	–	–	–	0.2652	0.5077	3.6469	0.5147	1,516.4	1,559.8	1,619.1	0.99	7.44	1.30	515.48
r13	A,4	–	–	–	–	0.2675	0.3707	3.7841	0.4183	1,528.3	1,589.4	1,671.3	0.89	9.10	1.30	398.33
05SG05 rutile																
r1	3	223	359	104.3	17.8	0.1817	0.0923	2.1132	0.1081	1,076.1	1,153.1	1,300.9	0.86	10.92	1.00	86.32
r3	3	266	426	81.5	14.4	0.1841	0.0629	2.1130	0.0844	1,089.3	1,153.1	1,275.0	0.75	29.79	1.00	34.09
r4	3	258	270	63.5	11.5	0.1929	0.0502	2.2793	0.0722	1,137.0	1,205.9	1,331.5	0.70	4.27	1.00	110.23
r5	3	223	266	173.0	28.9	0.1768	0.0553	2.0586	0.0784	1,049.4	1,135.1	1,303.0	0.71	15.22	1.00	66.80
r6	3	161	265	46.3	7.7	0.1771	0.0671	1.9414	0.0960	1,051.2	1,095.5	1,184.7	0.72	4.94	1.00	65.86
r7	3	123	300	120.4	16.0	0.1430	0.0581	1.5056	0.0952	861.4	932.6	1,105.0	0.62	2.06	1.00	130.77
r9	2	80	160	107.4	14.5	0.1458	0.0517	1.4983	0.1222	877.5	929.7	1,055.6	0.52	0.83	0.83	75.54
r11	1	40	150	46.8	5.0	0.1165	0.1440	1.0891	0.8610	710.5	748.1	862.2	0.53	0.51	0.51	9.30
r12	1	50	100	77.9	8.9	0.1233	0.0699	1.2279	0.4242	749.4	813.4	992.8	0.56	0.79	0.79	17.74
r13	2	50	170	25.2	2.9	0.1271	0.0797	1.2341	0.4456	771.1	816.2	941.1	0.50	0.70	0.70	18.66
r14	2	80	210	123.5	15.6	0.1368	0.0475	1.3747	0.0985	826.4	878.2	1,011.2	0.54	0.49	0.49	126.42
r15	2	70	150	1,237.1	184.5	0.1612	0.0447	1.7037	0.0783	963.5	1,009.9	1,112.0	0.61	0.55	0.55	166.75
r18	2	40	120	65.8	7.0	0.1145	0.2704	1.1308	1.1256	699.0	768.1	974.7	0.45	0.59	0.59	8.63
r19	2	45	200	81.9	9.5	0.1264	0.1779	1.2307	0.7753	767.2	814.7	946.6	0.48	0.61	0.61	11.70
r20	2	50	135	80.8	10.0	0.1341	0.4779	1.3709	0.5984	811.1	876.5	1,045.7	0.83	0.54	0.54	24.39
r24	1	20	130	80.0	16.6	0.1057	0.3461	0.9376	2.9328	647.5	671.6	753.5	0.59	1.10	1.09	3.34
r25	1	25	200	60.0	5.7	0.1037	0.3745	0.9749	3.3111	636.2	691.0	873.7	0.67	0.83	0.83	2.41
r27	1	40	120	65.4	7.3	0.1221	0.2332	1.2205	1.2537	742.7	810.0	999.8	0.52	1.82	1.00	3.33
r28	1	35	120	69.0	7.0	0.1111	0.3320	1.0814	1.8469	679.3	744.3	945.2	0.52	1.14	1.00	3.86
r29	2	45	155	71.8	8.2	0.1240	0.1025	1.2324	0.6430	753.3	815.4	988.9	0.57	0.91	0.91	11.72
r21	A,3	–	–	–	–	0.1653	0.0623	1.7521	0.0971	986.3	1,027.9	1,117.6	0.66	0.50	0.49	183.36
r22	A,3	–	–	–	–	0.1655	0.0919	1.7587	0.1146	987.4	1,030.4	1,122.7	0.81	11.15	1.00	47.68
r23	A,3	–	–	–	–	0.1593	0.0530	1.6788	0.0772	953.0	1,000.5	1,106.2	0.70	2.23	1.00	143.95
Redg1	E,1	–	–	–	–	0.0076	18.2119	0.0774	176.0267	48.9	75.7	1,032.0	0.75	0.66	0.66	0.05
Redg2	E,1	–	–	–	–	0.0117	17.7851	0.0927	131.3821	75.2	90.0	504.1	0.52	1.28	1.00	0.07
Redg4	E,1	–	–	–	–	0.0101	3.1316	0.0692	26.0069	64.7	67.9	184.3	0.53	0.93	0.90	0.41
05SG20 rutile																
r1	2	165	200	3.17	0.17	0.0612	0.2512	0.5608	2.6081	382.7	452.1	822.4	0.64	3.32	0.70	1.64
r2	2	240	265	9.42	0.60	0.0703	0.1623	0.6499	1.1133	438.0	508.4	839.3	0.53	3.64	0.70	3.36

Table 2 continued

Fractions	Grain descr.	Grain size (μm) Concentration (ppm)				206Pb/ 238U	% err	207Pb/ 235U	% err	Age (Ma)			Corr. coef.	Common est. Pb		
		w	l	U	Pb*					206 Pb/ 238 U	207 Pb/ 235 U	207 Pb/ 206 Pb		Pb (pg)	Blank (pg)	Pb*/ Pbc
r3	2	150	270	4.30	0.23	0.0584	0.1545	0.5339	1.2243	365.9	434.4	815.7	0.53	3.13	0.70	2.24
r5	2	200	300	1.77	0.10	0.0605	0.1761	0.5699	1.0208	378.7	457.9	878.3	0.49	2.51	0.70	2.78
r6	2	160	230	2.07	0.07	0.0392	0.3034	0.3157	2.7291	247.9	278.6	545.5	0.56	2.05	0.70	1.79
r7	2	150	300	2.49	0.07	0.0331	0.4135	0.2836	3.7378	209.9	253.5	679.2	0.59	2.51	0.70	0.92
r8	2	150	300	4.46	0.22	0.0562	0.2179	0.5291	2.1264	352.6	431.2	876.0	0.67	5.64	0.70	1.26
r11	2	150	220	0.65	0.03	0.1148	1.0451	1.0762	3.2525	700.3	741.8	869.0	0.48	3.57	0.70	1.14
r12	3	150	170	–	–	0.0599	1.2739	0.5474	8.8433	375.3	443.3	813.5	0.53	1.23	0.70	0.60
r14	3	150	150	–	–	0.0216	3.7176	0.2166	25.7215	137.5	199.1	1,010.6	0.56	1.40	0.70	0.18
r15	3	75	150	–	–	0.0454	1.6125	0.4136	17.2343	286.3	351.4	808.1	0.72	2.38	0.70	0.31

Grain morphology: *A* = abraded, *E* = isolated grain rim, *1* = euhedral, red, translucent, *2* = euhedral to subhedral, red to black, portions translucent, *3* = subhedral to anhedral, black

Pb* Radiogenic lead

range of sizes recorded from dated grains using diffusion kinetics from Cherniak (2000). Zircon U-Pb analyses and geothermometry constrain the model start time/temperature to 1,800 Ma/900°C for these samples. Model calculations for reheating paths that attempt to fit rutile data from MHB are presented in Fig. 10a. For this end-member t-T path the shallowest sample, 05SG02, would have had to cool quickly through the Pb PRZ at 1,800 Ma and been reheated at 800 Ma. Deeper samples 05SG05 and 05SG20 can be fit by similar paths with each quenching and reheating events occurring at different and younger times. As in the modeled data presented in Fig. 1a, the topology of the modeled data is a straight line between the timing of the initial cooling and the subsequent reheating event. Unlike the singular lower intercept produced during the reheating of multiple samples of variable depth test presented in Fig. 6b, these data could only be explained by multiple reheating events, each with is own resolvable lower intercept. This model has an additional requirement that each individual thermal event remain thermally isolated from the samples of different depths.

Forward calculated U-Pb data from slow cooling t-T paths can also be fit to each sample from Sweetgrass (Fig. 10b–d). To make systematic modeling easier, exponential cooling paths are approximated as segmented linear cooling paths. Several cooling rates through the rutile Pb PRZ are then tested to bracket the array of measured data. Each sample from Sweetgrass cools through the Pb PRZ at rates lower than 0.25°C/Ma with the shallowest sample cooling first and the deepest sample cooling last. The modeled data for each sample consists of a discordant array of data with an upper and lower intercept that is resolvable from the other samples. The topology of the modeled data is curvilinear and becomes asymptotic as it approaches concordia.

Discussion

Each rutile U-Pb dataset can be approximated with modeled data produced from reheating and slow cooling time-temperature paths (Fig. 10) and suggests the interpretation of data would be aided by a more general analysis of data trends. Though reheating t-T paths can roughly fit the data, this model requires discrete quenching and heating events throughout the history of the lithosphere (Fig. 10a inset). Zircon U-Pb data from these xenoliths as well as previous U-Pb zircon data from the region record only one significant thermotectonic event: the formation of the GFTZ at ~1.8 Ga (Table 1), (Bolhar et al. 2007; Davis and Ross 1999; Gorman et al. 2002). There are no geochronologic data within these xenoliths or from regional surface exposures that record high temperature events coincident in time with the lower intercepts from samples 05SG02 and 05SG05 (~800 and 500 Ma respectively). Furthermore, the reheating model would require that each individual event is large enough to cause significant loss of Pb within one sample yet remain thermally insulated from the samples above and below. This is inconsistent with the expectations for a multi-sample approach (Fig. 6b), where reheating events resulted in samples from different depths sharing a common lower intercept as a result of reheating.

We can also evaluate the fit of the modeled slow cooling t-T paths to the data. Each sample U-Pb data set defines a curvilinear array that is asymptotic to concordia, consistent with the expected topology of data for slow cooling

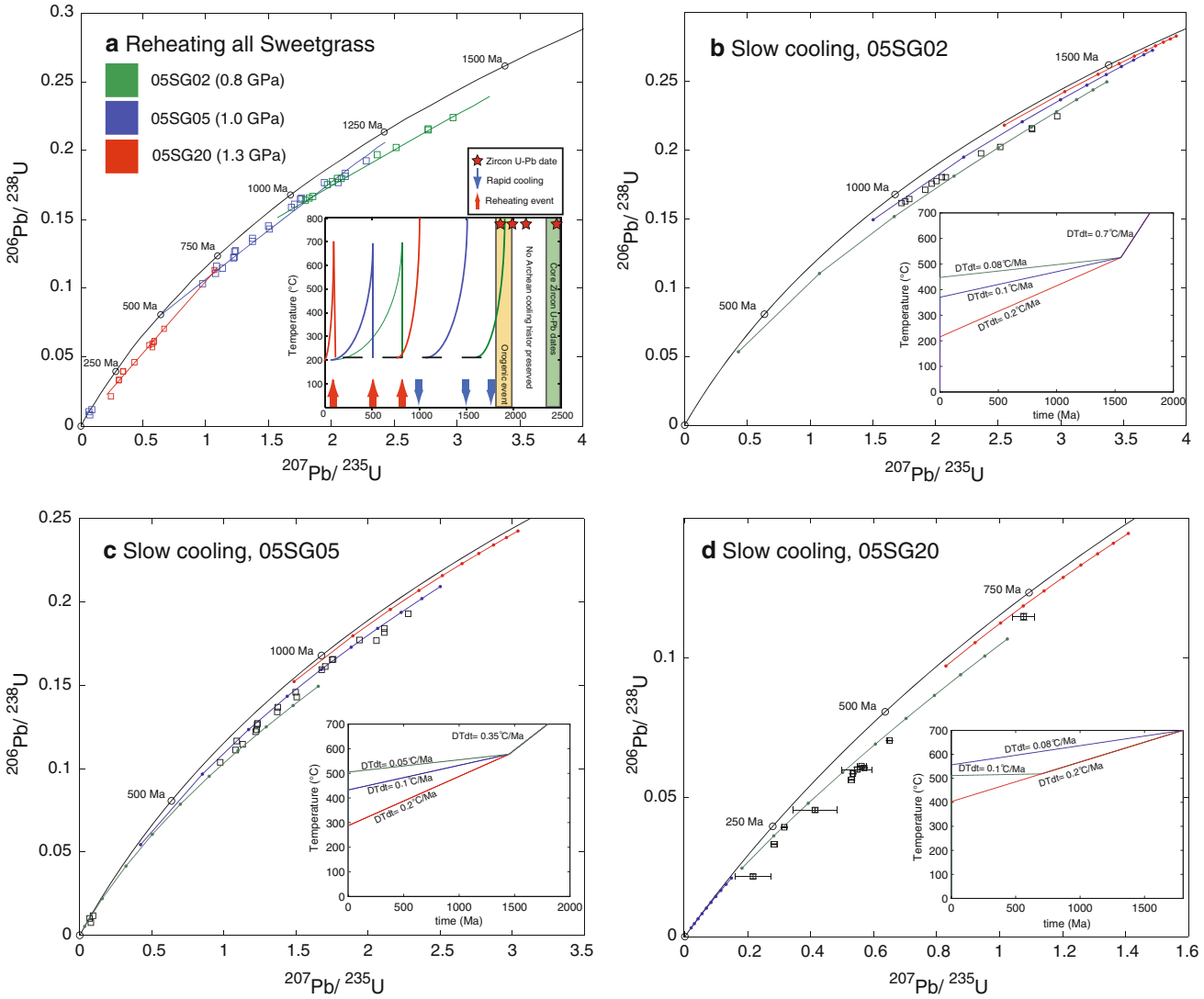

Fig. 10 Concordia plots showing a comparison between measured U-Pb data from lower crustal samples from the Sweetgrass volcanics (MHB) and forward calculated data assuming **a** reheating paths and **b–d** slow cooling paths

samples. Each array of data can be well-bracketed with model data with the same curvilinear trajectory and asymptotic curvature (Fig. 10 b–d). When we consider the 3 data sets as a whole the most important trend is the correlation between U-Pb dates for each xenolith and it's estimated residence depth. The simplest way to explain this trend is that these samples all record the progressive relaxation of a post-orogenic geothermal gradient. At ~1.8 Ga during the orogenic event, this geothermal gradient was sufficiently high to prevent lead retention in rutile from all depths. As the lithosphere cooled, the shallowest sample first entered the rutile PRZ, the timing of which is marked by the sample's upper intercept. The upper intercept of the shallowest sample (~1,800 Ma) is coincident with $^{40}Ar/^{39}Ar$ biotite and amphibole dates from nearby surface exposures (Holm and Schneider 2002). This is interpreted to indicate that temperatures within the MHB at ~25 km depth were <500°C shortly after the collision event. The next deepest sample, 05SG05 cooled to the top of its PRZ by ~1.5 Ga. Finally the deepest sample 05SG20 began to retain Pb by ~1.0 Ga. In the slow cooling model, the lower intercepts of each data set records the samples' exit from the rutile Pb PRZ. The coincidence of the lower intercept of 05SG20 with the age of the kimberlite is significant, as it marks the exhumation of the xenolith from within the rutile PRZ onto the Earth's surface where it was quenched. This also indicates that the crust at this depth was 450 ± 50°C at ~50 Ma. The trend of overlapping data previously modeled in Fig. 6a is also observed within the rutile data from the MHB, suggesting that the slow cooling recorded by each sample occurred at a comparable rate. The slow-cooling model does not require

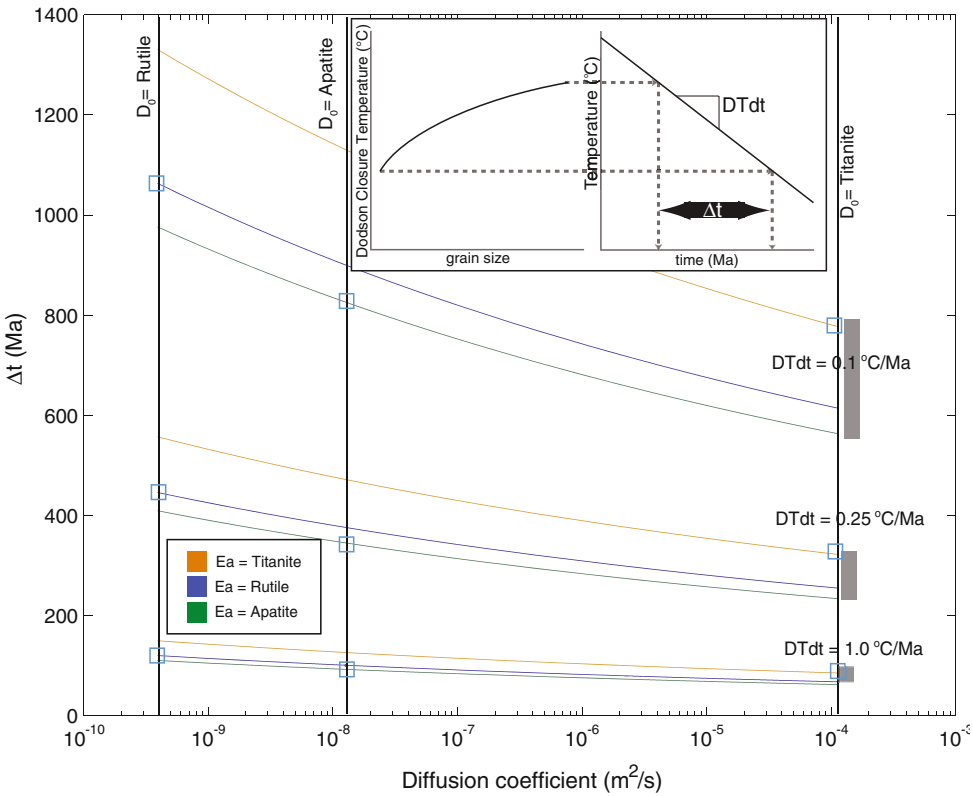

Fig. 11 Dodson equation calculated difference in time between small and large diffusion domains (Δt) over a range of diffusion coefficients, activation energies (E_a) and cooling rates (DTdt). Boxes are placed at the intersection of E_a and D_0 for each phase, marking the Δt at a particular cooling rate for that phase. The Dodson analytical solution provides a rapid way to test how sensitive the size of the Pb partial retention zone is to diffusion kinetics

temporally discrete quenching or reheating events and the trends within the data can be explained by a simple model for lithospheric thermal evolution. In the following section we will try to define an upper limit to the cooling rate for these samples by exploring the relationship between data topology and diffusion kinetics.

Data topology and the effects of diffusion kinetics

In a slowly cooled system, the degree of discordance in the U-Pb system is controlled by the cooling rate through PRZ. The extent of the PRZ in time-temperature space, based on numerical modeling (Fig. 5), is fairly insensitive to the diffusion kinetics. Further exploration of the relationship between PRZ residence time and diffusion kinetics can be made using the Dodson solution for closure temperature (Dodson 1973). This analytical solution provides a rapid way to evaluate how variation in diffusion kinetics affects the duration of partial system behavior; the later of which is roughly approximated by the difference in time (Δt) between the largest and smallest grain sizes for a particular cooling rate (Fig. 11). At the slow cooling rates we are examining, the absolute values of Δt predicted by the Dodson solution are inaccurate, as the solution does not accurately account for exponential Pb production by radiogenic decay. However, for our purpose of examining the *trends* between variable diffusion kinetics and the extent of partial system behavior, the Dodson solution is suitable. At cooling rates of 1.0°C/My and faster, the size of the PRZ is nearly completely insensitive to diffusion kinetics, yielding comparable Δt's for all combinations of kinetic values (Fig. 11). At cooling rates slower than 1.0°C/My, diffusion kinetics have an increased though second order effect on the size of the PRZ. For example, at a rate of 0.25°C/My, the entire range of Pb activation energies and diffusion coefficients yields a ~50% maximum range of Δt's, while decreasing the cooling rate from 0.25 to 0.1°C/My would change the Δt over 200%. At cooling rates as low as 0. 1°C/My, the range of the PRZ becomes highly sensitive to diffusion kinetics, thus decreasing our ability to conclude on a cooling rate a this range. At cooling rates between 1 and 0.25°C/My relative independence between diffusion kinetics and the size of the PRZ suggests that the topology of rutile U-Pb data alone can be used to place an upper limit to the cooling rate through the minerals' PRZ.

Though one cannot accurately model the exact temperatures of Pb retention in rutile without accurate diffusion kinetics, U-Pb data does confirm that rutile is obeying volume diffusion behavior based on the grain size dependencies in measured U-Pb dates, in particular the high quality grains from sample 05SG05 and 05SG02 (Fig. 9). Combining the empirical constraints on rutile Pb closure (Fig. 8) and a demonstration of cooling rate dependent data

topology that is relatively insensitive to diffusion kinetics (Figs. 5 and 11) allows for the conclusion that the cooling rate for samples from the Sweetgrass hills, through the rutile thermal window (450 ± 50°C) is on the order of 0.25°C/My or less.

Thermal state recorded by lower crustal thermochronometers

We can evaluate the thermal/tectonic state and mechanism of cooling within the lithosphere through a comparison of both the absolute temperatures recorded by the lower crustal thermochronometers and those predicted by physical models for heat transfer in the lithosphere (Ehlers et al. 2005). One of the most broadly applicable lithosphere thermal models is a stratified 1-D calculation, first described by (Pollack and Chapman 1977), that extrapolates the measured surface heat flux to the rest of the lithosphere while stripping out the internal heat contribution from the crust, lower crust and lithospheric mantle. This model allows us to test the sensitivity of lower crustal temperatures to any model parameter and explore a possible range of lower crustal temperatures. The assumed surface heat flux in this calculation has the most significant effect on lower crustal temperatures, with temperatures at 40 km depth ranging between 380°C on a cratonic geotherm (40mW/m^2) to over 800°C at a high geothermal gradient (80mW/m^2) (Chapman 1986). Other influential parameters include the distribution and concentration of heat producing elements (HPE) within the crust (Rudnick et al. 2003, 1998), thermal conductivity and Moho depth. Realistic variations in each of these parameters can cumulatively effect the temperature at 40 km depth by over 10%, yielding a range of lower crustal temperatures between 380 and 450°C for a cratonic geotherm (40mW/m^2) (Chapman 1986). These temperatures predicted for the low cratonic geothermal gradient are well within the temperatures of rutile Pb retention.

Conclusions

We have demonstrated how U-Pb thermochronology can be used to resolve unique time-temperature paths for lower crustal rocks exhumed by volcanic eruptions. Numerical solutions to the diffusion equation provide us with the means to exploring the U-Pb thermochronologic system's dependencies on: (1) grain size, (2) decay rate (^{238}U vs. ^{235}U), (3) cooling rate through the partial retention zone (PRZ) and (4) sensitivity to diffusion kinetics.

1. The length scale dependency of Pb diffusion causes grains of variable size to each have its own unique zone of Pb retention in time-temperature space. This results in grains of one size to retain a different Pb isotopic composition (produced by the decay of a different composition of parent U) than a grain of any other size.
2. The dramatically different decay rates for ^{238}U and ^{235}U are manifested in two ways. First, because the PRZ of any system is dependent upon production rate, the ^{235}U-^{207}Pb and ^{238}U-^{206}Pb systems each have their own PRZ. The higher production rate of ^{207}Pb leads to a relative excess in retained ^{207}Pb. Second, the difference in ^{238}U and ^{235}U decay constants yields time sensitive information on Pb diffusion that can be utilized for resolving the difference between reheating and slow-cooling events. Reheating time-temperature paths lie along a straight line between the time of initial quenching and the subsequent thermal event. Slow cooling t-T paths yield an asymptotic topology of data for multiple analyses of variable grain size.
3. The topology of data produced by slow cooling t-T paths is strongly dependent upon cooling rate through the PRZ. Longer durations yield longer more discordant arrays of data providing a tool for estimating the cooling rate through the PRZ.
4. The topology of this variable grain size data is generally insensitive to kinetics in comparison to cooling rate, allowing users to estimate cooling rate for minerals with poorly constrained diffusion kinetics.

In the Montana study area, rutile U-Pb data from three xenoliths derived from different depths from a single volcanic epicenter are best interpreted by slow cooling t-T paths where the shallowest sample cooled first and the deepest last. Combining the topological dependence of U-Pb data on cooling path with the multiple sample of variable depth approach supports the conclusion that lower crustal thermochronometers record a slow thermal relaxation since the Paleoproterozoic. Comparing the rates predicted by these thermochronologic results with the rates predicted for physical models of heat transfer within the earth will allow future studies to evaluate the mechanisms for cooling and heat transfer within the lithosphere.

Acknowledgments Primary funding for this project was provided through EarthScope grant EAR- 0746205. The authors would like to thank D. Canil and F. Corfu for their constructive reviews and Timothy Grove for his editorial handling. Discussions throughout this study with both Doug Walker and Noah McLean were insightful and greatly appreciated.

References

Anderson SD, Jamieson RA, Reynolds PH, Dunning GR (2001) Devonian extension in northwestern Newfoundland: 40Ar/39Ar

and U‘ÄêPb data from the ming‘äôs bight area, baie verte peninsula. J Geol 109(2):191–211
Baldwin J, Bowring SA, Williams ML, Williams IS (2004) Eclogites of the Snowbird tectonic zone: petrological and U-Pb geochronological evidence for Paleoproterozoic high-pressure metamorphism in the western Canadian Shield. Contrib Mineral Petrol 147:528–548
Berman RG (1991) Thermobarometry using multi-equilibrium calculations; a new technique, with petrological applications; quantitative methods in petrology; an issue in honor of Hugh J. Greenwood. Can Mineral 29:833–855
Berman RG (2007) winTWQ (version 2.3): a software package for performing internally consistent thermobarometric calculations. In: Geological survey of canada open file report 5462, p 41
Bolhar R, Kamber BS, Collerson KD (2007) U-Th-Pb fractionation in Archaean lower continental crust: implications for terrestrial Pb isotope systematics. Earth Planet Sci Lett 254:127–145
Canil D, Fedortchouk Y (1999) Garnet dissolution and the emplacement of kimberlites. Earth Planet Sci Lett 167(3–4):227–237
Chapman DS (1986) Thermal gradients in the continental crust. Geol Soc London Spec Publ 24(1):63–70
Cherniak DJ (1993) Lead diffusion in titanite and preliminary results on the effects of radiation damage on Pb transport. Chem Geol 110(1–3):177–194
Cherniak DJ (2000) Pb diffusion in rutile. Contrib Mineral Petrol 139:198–207
Cherniak DJ, Watston EB (2001) Pb diffusion in zircon. Chem Geol 172(1):5–24
Cherniak DJ, Lanford WA, Ryerson FJ (1991) Lead diffusion in apatite and zircon using ion implantation and Rutherford Backscattering techniques. Geochim Cosmochim Acta 55(6):1663–1673
Connolly JAD, Petrini K (2002) An automated strategy for calculation of phase diagram sections and retrieval of rock properties as a function of physical conditions. J Metamorph Geol 20:267–708
Corfu F, Easton RM (2001) U-Pb evidence for polymetamorphic history of Huronian rocks within the Grenville front tectonic zone east of Sudbury, Ontario, Canada. Chem Geol 172(1–2):149–171
Corfu F, Stone D (1998) The significance of titanite and apatite U-Pb ages: constraints for the post-magmatic thermal-hydrothermal evolution of a batholithic complex, Berens River area, northwestern Superior Province, Canada. Geochim Cosmochim Acta 62(17):2979–2995
Crank J (1956) Mathematics of diffusion. Clarendon Press, Oxford
Davis WJ, Ross GM (1999) Proterozoic underplating of the Archean wyoming craton and medicine hatt block during Assembly of Western Laurentia. Ninth annual V.M. Goldschmidt conference
Davis WJ, Berman R, Kjarsgaard B (1995) U-Pb geochronology and isotopic studies of crustal xenoliths from the Archean Medicine Hat block, northern Montana and southern Alberta: paleoproterozoic reworking of Archean lower crust. In: Ross GM (ed) Alberta basement transects: lithoprobe report #47, pp 329–334
Davis WJ, Canil D, MacKenzie JM, Carbno GB (2003) Petrology and U-Pb geochronology of lower crustal xenoliths and the development of a craton, Slave Province, Canada. Lithos 71:541–573
Dodson MH (1973) Closure temperature in cooling geochronological and petrological systems. Contrib Mineral Petrol 40:259–274
Edgar AD, Arima M, Baldwin DK, Bell DR, Shee SR, Skinner EMW, Walker EC (1988) High-pressure-high-temperature melting experiments on a SiO 2 -poor aphanitic kimberlite from the Wesselton Mine, Kimberley, South Africa. Am Mineral 73:524–533
Eggler DH, Wendlandt E (1979) Experimental studies on the relationship between kimberlite magmas and partial melting of peridotite. In: Boyd FR, Meyer HOA (eds) Kimberlites, diatremes, and diamonds: their geology petrology and geochemistry. American Geophysical Union, Washington, pp 330–338
Ehlers TA, Chaudhri T, Kumar S, Fuller CW, Willett SD, Ketcham R, Brandon MT, Belton D, Kohn B, Gleadow AJ, Dunai T, Fu F (2005) Computational tools for low-temperature thermochronometer interpretation. Rev Mineral Geochem 58:589–622
Esperanca S, Holloway JR (1987) On the origin of some mica-lamprophyres: experimental evidence from a mafic minette. Contrib Mineral Petrol 95(2):207–216
Ferry J, Watson E (2007) New thermodynamic models and revised calibrations for the Ti-in-zircon and Zr-in-rutile thermometers. Contrib Mineral Petrol 154(4):429–437
Flowers RM, Mahan KH, Bowring SA, Williams ML, Pringle MS, Hodges KV (2006) Multistage exhumation and juxtaposition of lower continental crust in the western Canadian Shield: linking high-resolution U-Pb and 40Ar/39Ar thermochronometry with pressure-temperature-deformation paths. Tectonics 25(4):TC4003
Giletti BJ (1974) Studies in diffusion I: Argon in phlogopitic mica. In: Hoffman AW, Giletti BJ, Yoder HS, Yund RA (eds) Geochemical transport and kinetics, vol 634. Carnegie Institute of Washington, Washington, DC, pp 107–115
Gorman AR, Clowes RM, Ellis RM, Henstock TJ, Spence GD, Keller RG, Levander A, Snelson CM, Burianyk M, Kanasewich ER, Asudeh I, Hajnal Z, Miller KC (2002) Deep Probe: imaging the roots of western North America. Can J Earth Sci 39(3):375
Hames WE, Bowring SA (1994) An empirical evaluation of the argon diffusion geometry in muscovite. Earth Planet Sci Lett 124(1–4):161–169
Harrison TM (1982) Diffusion of 40Ar in hornblende. Contrib Mineral Petr 78(3):324–331
Heizler M (2002) Slow-cooling or reheating: can SW USA thermochronological data be reconciled? In: Geological Society of America, vol 80–4. Denver
Hodges KV, Bowring SA (1995) 40Ar/39Ar thermochronology of isotopically zoned micas: Insights from the southwestern USA proterozoic orogen. Geochim Cosmochim Acta 59(15):3205–3220
Holm D, Schneider D (2002) 40Ar/39Ar evidence for ca. 1800 Ma tectonothermal activity along the Great Falls tectonic zone, central Montana. Can J Earth Sci 39(12):1719
Jaffey AH, Flynn KF, Glendenin LE, Bentley WC, Essling AM (1971) Precision measurement of half-lives and specific activities of ^{235}U and ^{238}U. Phys Rev C 4(5):1889
Jordan TH (1988) Structure and formation of the cotinental tectosphere. J Petrol 1:11–37
Mattinson JM (2005) Zircon U-Pb chemical abrastion (“CA-TIMS”) method: combined annealing and multi-step partial dissolution analysis for improved precision and accuracy of zircon ages. Chem Geol 220:47–66
Mezger K, Hanson GN, Bohlen SR (1989) High-precision U-Pb ages of metamorphic rutile: application to the cooling history of high-grade terranes. Earth Planet Sci Lett 96:106–118
Miller BV, Dunning GR, Barr SM, Raeside RP, Jamieson RA, Reynolds PH (1996) Magmatism and metamorphism in a Grenvillian fragment: U-Pb and 40Ar/39Ar ages from the Blair River Complex, Northern Cape Breton Island, Nova Scotia, Canada. Geol Soc Am Bull 108(2):127–140
Moller A, Mezger K, Schenk V (2000) U-Pb dating of metamorphic minerals: Pan-African metamorphism and prolonged slow cooling of high pressure granulites in Tanzania, East Africa. Precambrian Res 104(3–4):123–146
Morin D, Corriveau L (1996) Fragmentation processes and xenolith transport in a Proterozoic minette dyke, Grenville province, Quebec. Contrib Mineral Petrol 125(4):319–331
Mueller PA, Heatherington AL, Kelly DM, Wooden JL, Mogk D (2002) Paleoproterozoic crust within the Great Falls tectonic

zone: implications for the assembly of southern Laurentia. Geology 30(2):127–130

Mueller PA, Burger HR, Wooden JL, Brady JB, Cheney JT, Harms TA, Heatherington AL, Mogk DW (2005) Paleoproterozoic metamorphism in the northern wyoming province: implications for the assembly of laurentia. J Geol 113:169–179

Pollack HN, Chapman DS (1977) On the regional variation of heat flow, geotherms, and lithospheric thickness. Tectonophysics 38:279–296

Rudnick RL, McDonough WF, O'Connell RJ (1998) Thermal structure, thickness and composition of continental lithosphere. Chem Geol 145(3–4):395–411

Rudnick RL, Gao S, Heinrich DH, Karl KT (2003) Composition of the continental crust. In: Treatise on geochemistry. Pergamon, Oxford, pp 1–64

Rutherford MJ (2008) Magma Ascent Rates. In: Putirka KD, Tepley FJ (eds) Minerals, inclusions and volcanic processes, vol 69. Mineralogical Society of America, Washington, pp 241–271

Schmitz MD, Bowring SA (2003) Constraints on the thermal evolution of continental lithosphere from U-Pb accessory mineral thermochronometry of lower crustal xenoliths, southern Africa. Contrib Mineral Petrol 144:592–618

Schoene B, Bowring SA (2007) Determining accurate temperature-time paths from U-Pb thermochronology: An example from the Kaapvaal craton, southern Africa. Geochim Cosmochim Acta 70:165–185

Sparks RSJ, Baker L, Brown RJ, Field M, Schumacher J, Stripp G, Walters A (2006) Dynamical constraints on kimberlite volcanism. J volcanol Geotherm Res 155(1–2):18–48

Spera FJ (1984) Carbon dioxide in petrogenesis III: role of volatiles in the ascent of alkaline magma with special reference to xenolith-bearing mafic lavas. Contrib Mineral Petrol 88(3):217–232

Tilton GR (1960) Volume diffusion as a mechanism for discordant lead ages. J Geophys Res 65(9):2945–2963

Villeneuve ME, Ross GM, Theriault RJ, Miles W, Parrish RR, Broome J (1993) Tectonic subdivision and U-Pb geochronology of the crystalline basement of the Alberta Basin, Western Canada. Geol Surv Can Bull 447:86

Watson E, Wark D, Thomas J (2006) Crystallization thermometers for zircon and rutile. Contrib Mineral Petrol 151(4):413–433

Wetherill G (1956) Discordan Uranium-Lead ages, I. Transactions. Am Geophys Union 37(3):320–326

Whitney DL, Evans BW (2010) Abbreviations for names of rock-forming minerals. Am Mineral 5(1):185–187